m^{6}A RNA methylation regulates the fate of endogenous retroviruses

https://doi.org/10.1038/s41586-020-03135-1

Received: 4 March 2020

Accepted: 30 November 2020

Published online: 13 January 2021

Check for updates

Tomasz Chelmicki[1]✉, Emeline Roger[1], Aurélie Teissandier[1], Mathilde Dura[1], Lorraine Bonneville[1], Sofia Rucli[1], François Dossin[2], Camille Fouassier[3], Sonia Lameiras[4] & Deborah Bourc'his[1]✉

Endogenous retroviruses (ERVs) are abundant and heterogenous groups of integrated retroviral sequences that affect genome regulation and cell physiology throughout their RNA-centred life cycle[1]. Failure to repress ERVs is associated with cancer, infertility, senescence and neurodegenerative diseases[2,3]. Here, using an unbiased genome-scale CRISPR knockout screen in mouse embryonic stem cells, we identify m^{6}A RNA methylation as a way to restrict ERVs. Methylation of ERV mRNAs is catalysed by the complex of methyltransferase-like METTL3–METTL14[4] proteins, and we found that depletion of METTL3–METTL14, along with their accessory subunits WTAP and ZC3H13, led to increased mRNA abundance of intracisternal A-particles (IAPs) and related ERVK elements specifically, by targeting their 5′ untranslated region. Using controlled auxin-dependent degradation of the METTL3–METTL14 enzymatic complex, we showed that IAP mRNA and protein abundance is dynamically and inversely correlated with m^{6}A catalysis. By monitoring chromatin states and mRNA stability upon METTL3–METTL14 double depletion, we found that m^{6}A methylation mainly acts by reducing the half-life of IAP mRNA, and this occurs by the recruitment of the YTHDF family of m^{6}A reader proteins[5]. Together, our results indicate that RNA methylation provides a protective effect in maintaining cellular integrity by clearing reactive ERV-derived RNA species, which may be especially important when transcriptional silencing is less stringent.

Mammalian genomes host millions of retrotransposons, including ERVs that derive from past retroviral infections and have integrated as permanent residents. Over the course of evolution, successive waves of ERVs have multiplied and diversified, providing a fertile ground for genomic innovations. However, ERVs potentially compromise genomic integrity by disrupting genome structure and expression[6]. In laboratory mice, roughly 12% of pathological mutations result from ERV integrations, half of which emanate from a single family of the ERVK class, the IAPs, that comprise approximately 2,800 full-length copies[7]. By contrast, human ERVs are mostly transposition-defective[8]. However, by providing *cis*-regulatory modules, ERVs can also divert regulatory networks and alter cellular states. Moreover, ERVs generate RNA, cDNA, RNA–DNA hybrid species and proteins, the accumulation of which is associated with and may contribute to senescence, cancer and neurodegenerative diseases[3].

Homeostatic regulation of ERVs is achieved by surveillance at different steps of the ERV life cycle. Notably, chromatin-based silencing by DNA methylation and histone modifications and post-transcriptional control through RNA editing and RNA interference have extensively been characterized[9]. However, these control mechanisms are not active in all cell types or developmental periods. To identify unknown ERV-limiting factors, we performed a CRISPR–Cas9 loss-of-function screen for IAPEz control, a highly active mouse ERV. We engineered mouse embryonic stem (ES) cells to carry constitutively expressed Cas9 and a reporter cassette with IAPEz regulatory elements: IAPEz(5′LTR-UTR+3-60n *gag*)-GFP-Blast^R (Supplementary Table 1), in which 'LTR' denotes long terminal repeat and 'UTR' denotes the untranslated region (Fig. 1a, Extended Data Fig. 1a). Placing a doxycycline (dox)-responsive promoter upstream of the LTR sequence allowed us to test reactivation of the reporter after dox induction, to choose blasticidin-resistance over GFP as a more sensitive marker, and to adjust the blasticidin concentration for selection (Extended Data Fig. 1b, c). We also showed that the IAPEz reporter responded to known IAP repressors, by transducing cells with single guide RNAs (sgRNAs) against KAP1[10] (Extended Data Fig. 1d, e, Supplementary Fig. 1, Supplementary Tables 2, 3).

For the screen, we transduced IAPEz-reporter cells with a lentiviral genome-wide sgRNA library at multiplicity of infection (MOI) of 0.2–0.3 (Fig. 1b). The frequencies of sgRNAs after the application of blasticidin (5, 7 and 9 days) versus non-selected conditions were assessed via sequencing, and candidate genes were identified using MAGeCK (model-based analysis of genome-wide CRISPR–Cas9 knockout)[11]. Selection efficiency was verified by dropout of control intergenic sgRNAs, and genes were ranked on the basis of sgRNA *P* values (Fig. 1c, Supplementary Tables 4, 5). Several known IAP-repressing genes were among the top 100 hits: *Resf1*, *Trp53*, *Daxx*, *Atrx*, *Uhrf1*, *Cbx1* and *Dnmt1*[12–15]. Moreover, we identified several previously unknown candidates for IAP control (Supplementary Table 4). Notably, among the top hits were regulators of the *N*^{6}-methyladenosine (m^{6}A) mRNA methylation pathway, such as

[1]Institut Curie, PSL Research University, INSERM U934, CNRS UMR3215, Paris, France. [2]European Molecular Biology Laboratory, Heidelberg, Germany. [3]CRISPR'IT Genetic Platform Screening, Institut Curie, Paris, France. [4]ICGex Next-Generation Sequencing Platform, Institut Curie, PSL Research University, Paris, France. ✉e-mail: tomasz.chelmicki@curie.fr; deborah.bourchis@curie.fr

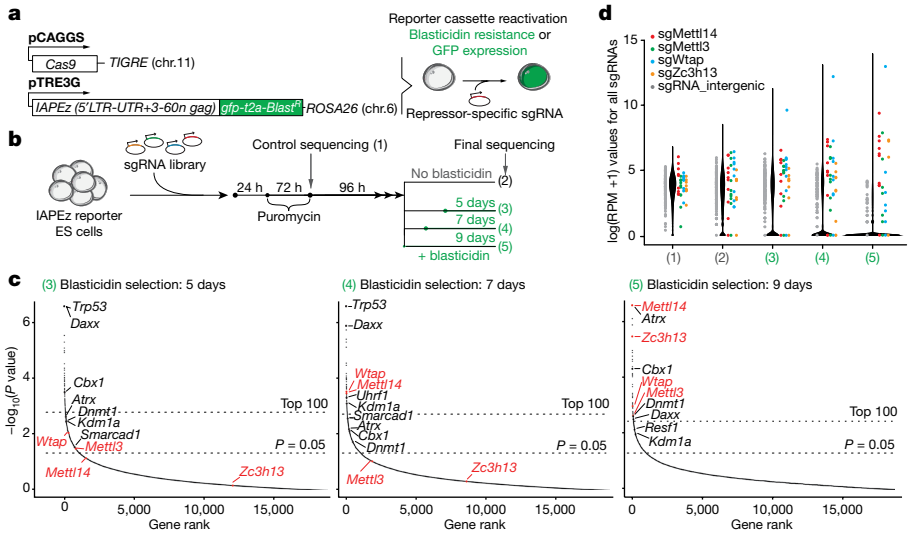

Fig. 1 | CRISPR screen for IAP suppressors in mouse ES cells. a, Schematic of the IAPEz reporter and experimental rationale. **b**, Workflow and timelines for the CRISPR–Cas9 knockout screen (screen I). **c**, Ranked *P* values (permutation test by MAGeCK[11]; Methods) for enriched genes after 5 (left), 7 (middle) and 9 (right) days of blasticidin treatment. Discontinued lines indicate genes ranked in top 100 according to *P* value (top) and $P = 0.05$ (bottom). Known IAP regulators (black, when $P < 0.05$) and *Mettl3*, *Mettl14*, *Wtap* and *Zc3h13* (red) are reported. **d**, Violin plots for all sgRNA read counts represented as the logarithm of reads per million (RPM) after library introduction (1), without selection (2) and after blasticidin selection (3–5); sgRNAs targeting *Mettl14* (sgMettl14; red, $n = 10$), *Mettl3* (sgMettl4; green, $n = 10$), *Wtap* (sgWtap; blue, $n = 10$), *Zc3h13* (shZc3h13; orange, $n = 9$) and intergenic sequences (sgRNA_intergenic; grey, $n = 199$).

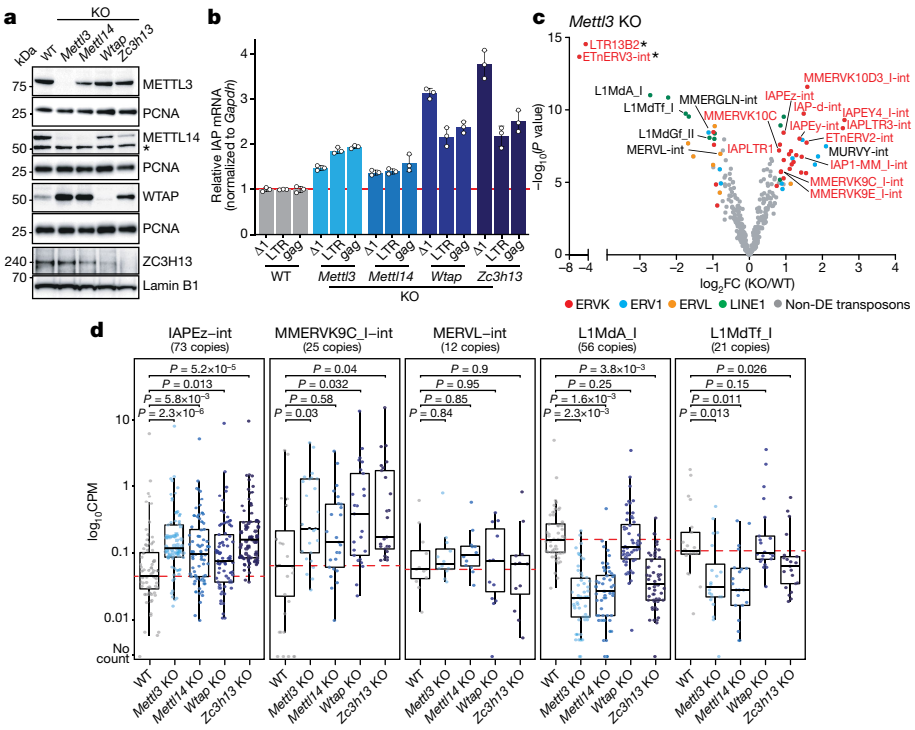

Fig. 2 | Depletion of the m^{6}A methyltransferase complex increases IAP mRNA levels. a, Immunoblot showing *Mettl3*, *Mettl14*, *Wtap* and *Zc3h13* knockout (KO) in ES cells. PCNA and lamin B1 served as loading controls; asterisk indicates unspecific band. Immunoblotting was repeated at least twice with similar results. **b**, RT–qPCR showing normalized IAP mRNA levels using primers against Δ1, LTR and *gag* sequences in the indicated knockouts relative to wild-type (WT) control (set to 1). Data are mean ± s.d. of three independent experiments. **c**, Volcano plot showing $\log_2$-transformed fold change ($\log_2$FC) in retrotransposon expression in *Mettl3* knockout versus wild-type control using random assignment of multi-mapped reads. Red, blue, orange and green denote significantly deregulated RepeatMasker annotations belonging to ERVK, ERV1, ERVL and L1 families, respectively. Grey denotes non-differentially expressed (non-DE) retrotransposons. *P* values were computed using limma and adjusted with the Benjamini–Hochberg correction (Methods). $\log_2$FC > 0.75; false discovery rate (FDR) < 0.05. **d**, Box plots showing expression ($\log_{10}$CPM; in which CPM denotes counts per million) of individual retrotransposon copies in wild-type and knockout ES cells. RNA-seq mapping allowed only unique hits in the reference genome and only copies with at least ten reads in at least one sample were conserved. Horizontal lines denote median, box limits correspond to upper and lower quartiles. *P* values determined by two-sided Student's *t*-test.

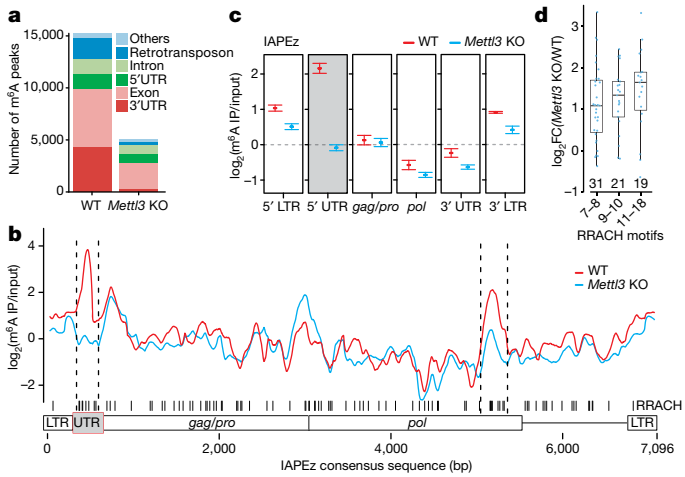

Fig. 3 | IAP mRNAs undergo m^{6}A methylation. a, Bar plot showing m^{6}A peaks within indicated genomic features. **b**, Average of input-normalized m^{6}A signal intensities along the IAPEz consensus sequence in wild-type (red) and *Mettl3* knockout (blue) cells. Vertical black lines denote RRACH motif positions. Discontinued vertical black lines delineate regions of m^{6}A enrichment present in wild-type cells and lost in *Mettl3*-knockout cells. **c**, Average of m^{6}A signal intensities for indicated IAPEz segments in wild-type (red) and *Mettl3*-knockout (blue) ES cells. Error bars indicate mean ± s.d. of three independent MeRIP-seq. **d**, Box plot showing $\log_2$FC in expression of uniquely mapped IAPEz copies grouped according to numbers of 5′ UTR-associated RRACH motifs in *Mettl3*-knockout versus wild-type cells. Box plots as in Fig. 2d. Only copies with a minimum of ten reads in at least one sample were conserved.

Mettl3, *Mettl14*, *Wtap* and *Zc3h13*, the enrichment of which gradually increased with extended blasticidin-mediated pressure (Fig. 1c, d). By repeating the screen under the most stringent selection, we confirmed significant enrichment for *Mettl3*, *Mettl14* and *Wtap* sgRNAs (Extended Data Fig. 2a, b). m^{6}A is the most abundant internal mark on mRNAs, and is crucial for organizing their fate—including export, decay and translation—in an array of biological processes such as development, cell differentiation, stress response and cancer[4]. The deposition of m^{6}A is exerted by a nuclear complex with an enzymatically active core formed by methyltransferase-like METTL3 and METTL14 proteins and other calibrating subunits, including WTAP and ZC3H13. METLL3 and METTL14 form a heterodimer, in which METTL3 is the catalytic component and METTL14 facilitates binding to the RNA substrate. WTAP and ZC3H13 are essential for assembling the complex into the nucleus[16,17].

To confirm that methylation of m^{6}A RNA regulates endogenous IAP copies, we generated individual ES cell lines that contained gene knockouts of *Mettl3*, *Mettl14*, *Wtap* and *Zc3h13* (Fig. 2a, Extended Data Fig. 3a–d). To avoid differentiation and lethality effects previously reported when m^{6}A-depleted ES cells are cultured in metastable conditions (serum plus leukaemia inhibitory factor (LIF)), we derived and cultured ES cells in a medium that stabilizes a ground state of pluripotency ('2i + LIF' medium)[18]. In these conditions, the identity of ES cells was globally preserved in the mutant lines (Extended Data Fig. 3e, f), with a mild reduction in proliferation (Extended Data Fig. 3g). We first confirmed reduced m^{6}A RNA methylation levels in the four knockout lines by enzyme-linked immunosorbent assay (ELISA) (Extended Data Fig. 4a). We used quantitative PCR with reverse transcription (qRT–PCR) to confirm that knockout of each of the four m^{6}A factors increased the abundance of endogenous IAPEz mRNA by two- to three-fold compared to wild-type cells (Fig. 2b). RNA sequencing (RNA-seq) analysis confirmed significant upregulation of IAPEz in m^{6}A mutants, as well as close relatives within the ERVK family—such as MMERVK10C, MMERVK10D3, ETnERV2 and Y chromosome-specific IAPEy elements—that share more than 65% sequence identity with IAPEz (https://www.dfam.org/) (Fig. 2c, Extended Data Fig. 4b–f, Supplementary Table 6). Specific Y-linked elements of the ERV1 family were also more abundant in the knockout lines (MuRVY). Upregulation of ERVK was observed at the subfamily level after random assignment of multi-mapped reads, and confirmed at the level of individual ERVK copies, when considering uniquely assigned reads only (Fig. 2d, Extended Data Fig. 5a). By contrast, MERVL remained globally unaffected and evolutionarily young long interspersed nuclear elements (LINEs or L1s) transcripts showed opposite downregulation in m^{6}A-knockout ES cells (Fig. 2c, d, Extended Data Figs. 4e, f, 5a). These different responses to the loss of m^{6}A mRNA methylation highlight the divergent effects that this pathway may exert depending on the retrotransposon type, with a negative effect on IAP-related ERVK elements, specifically. ERVK-specific upregulation was confirmed in published nuclear RNA-seq datasets from independent *Mettl3*-knockout ES cells[19] (Extended Data Fig. 5b).

We next evaluated the potential effect of increased IAP transcripts on gene regulation. As previously shown, hundreds of gene transcripts were upregulated in m^{6}A mutant ES cells[20], among which 941 were common between the 4 knockout lines (Extended Data Fig. 6a). However, these upregulated genes did not show correlation with proximity of ERVK annotations (−5 kb to +1 kb from the transcription start site (TSS)) (Extended Data Fig. 6b). Moreover, we did not score increased splicing between exonic sequences and IAP fragments in m^{6}A-knockout compared to wild-type ES cells (Extended Data Fig. 6c). As a whole, we conclude that the increased abundance of IAP transcripts after loss of m^{6}A loss minimal *cis*-effects on gene expression. Notably, depletion of m^{6}A did not result in downregulation of known retrotransposon repressors (Extended Data Fig. 6d) and did not alter ES cell identity, as demonstrated by expression levels of pluripotency and early differentiation genes (Extended Data Fig. 3e). This provides strong indication that m^{6}A RNA methylation directly represses IAP elements.

To verify this, we mapped the abundance and topology of m^{6}A methylation on IAPEz transcripts, by m^{6}A immunoprecipitation (methylated RNA immunoprecipitation sequencing (MeRIP–seq)) of total RNA from wild-type and *Mettl3*-knockout ES cells. We scored 15,216 and 4,864 m^{6}A peaks in wild-type and *Mettl3*-knockout ES cells, respectively, with substantially higher m^{6}A signal intensities in wild-type cells (Extended Data Fig. 7a). Notably, in addition to the well-characterized enrichment of m^{6}A methylation at the 3′ UTR and exons of genic mRNAs[20–23] (Fig. 3a, Extended Data Fig. 7b, c), we found that a considerable number of METTL3-dependent m^{6}A events mapped to retrotransposon annotations, comprising 13% of all peaks, including L1s—as recently reported[19,24]—and ERVK elements (Fig. 3a). When we plotted m^{6}A distribution along the IAPEz consensus sequence, we found two distinct regions of METTL3-dependent m^{6}A enrichment, predominantly at the 5′UTR—present in the IAPEz reporter—and to a lesser extent on the *Pol* sequence (Fig. 3b, c, Extended Data Fig. 7d). Enrichment in m^{6}A also coincided with the 5′ UTR region of MMERVK10C (Extended Data Fig. 7e, f) and was rather spread across L1MdA_I (Extended Data Fig. 7g, h). The m^{6}A RNA methylation mostly occurs on conserved RRACH sequence motifs (in which R denotes A or G, and H denotes A, C or U)[21,23]. Accordingly, we found several RRACH motifs on the 5′ UTR of IAPEz and MMERVK10C consensus sequences (Fig. 3b, Extended Data Fig. 7e, i). By focusing on uniquely mapped copies, we found that m^{6}A-dependent repression was proportional to the RRACH content: the more RRACH motifs an IAPEz copy contains in the 5′ UTR, the more upregulated it is in m^{6}A-knockout cells (Fig. 3d, Extended Data Fig. 7j). These data demonstrate for the first time, to our knowledge, that IAPs and their ERVK relatives undergo m^{6}A RNA methylation, and reveal a new pathway of retrotransposon suppression.

Functions of the m^{6}A RNA methylation complex have so far been investigated by conventional gene perturbation techniques—such as knockout or short hairpin RNA (shRNA)-mediated knockdown—which precludes examining the early consequences of m^{6}A loss and can also lead to secondary effects after prolonged selection. To address the early and direct IAP responses to m^{6}A depletion, we used auxin-inducible

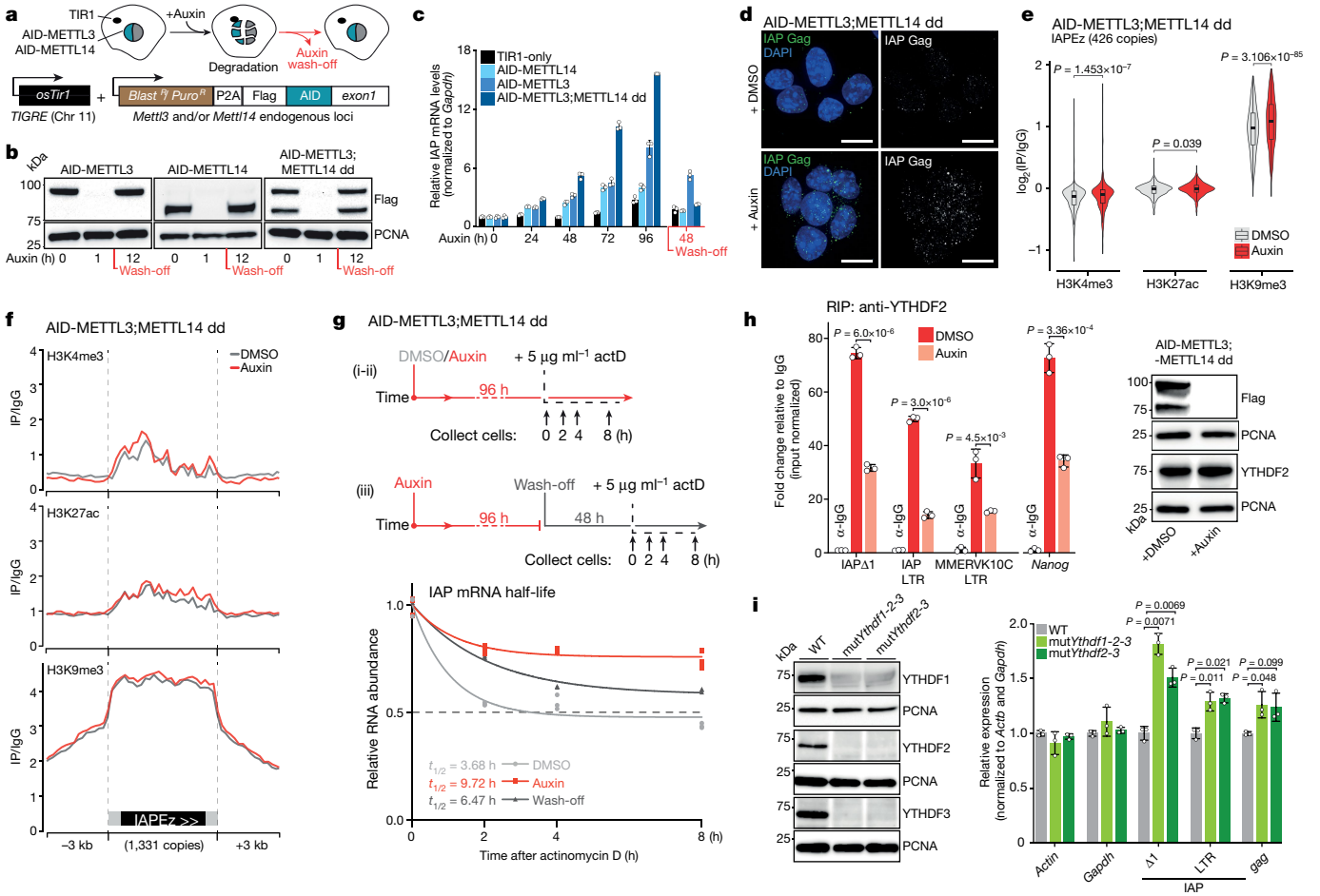

Fig. 4 | IAP chromatin status and RNA stability upon inducible degron of the m^{6}A methyltransferase complex. a, Schematic of METTL3 and METTL14 degron engineering. **b**, Immunoblot showing auxin-induced degradation of endogenous 3×Flag-AID-METTL3, -METTL14 and -METTL3;METTL4 double degron (dd). PCNA served as a loading control. **c**, RT–qPCR showing normalized IAP mRNA levels relative to 0h using LTR-specific primers after degron of METTL14 (light blue), METTL3 (blue) and METTL3;METTL14 dd (dark blue). TIR1-only (black) ES cells served as control. Error bars indicate mean ± s.d. of three independent auxin inductions. **d**, Immunofluorescence staining for IAP Gag in METTL3;METTL14 double degron after 96 h of treatment with DMSO (top) or auxin (bottom). Scale bar, 10 μm. **e**, Violin plots and box plots (inside) showing H3K4me3, H3K27ac and H3K9me3 levels at IAPEz copies (n = 426) determined by CUT&RUN in METTL3;METTL14 dd after 96 h of DMSO (grey) or auxin (red). Only copies with at least 10 reads in at least one sample were conserved. Box plots as in Fig. 2d. P values were determined by two-sided Student's t-test. **f**, Composite profiles showing H3K4me3 (top), H3K27ac (middle) and H3K9me3 (bottom) coverage along full-length (greater than 5 kb) IAPEz copies (n = 1,331) in METTL3;METTL14 double degron after 96 h of DMSO (grey) or auxin (red). **g**, Top, scheme for evaluating IAP mRNA degradation rates in METTL3;METTL14 double degron ES cells exposed to DMSO or auxin and actinomycin D (actD) for 2, 4 and 8 h before (i–ii) and after (iii) auxin wash-off. Bottom, relative IAP mRNA levels and half-life measurements in ES cells exposed to DMSO (light grey), auxin (red) and after auxin wash-off (dark grey) using Δ1-specific primers (n = 3 independent experiments). **h**, Left, YTHDF2 RIP-qPCR for ERVKs and *Nanog* in METTL3;METTL14 double degron cells after treatment for 96 h with DMSO (red) or auxin (pink). Rabbit IgG served as control. Data are mean ± s.d. of three independent experiments. P values were determined by two-stage linear step-up procedure of Benjamini, Krieger and Yekutieli. Right, immunoblot showing METTL3 and METTL14 (Flag), and YTHDF2 in METTL3;METTL14 double degron cells after treatment with DMSO or auxin for 96 h. PCNA served as loading control. **i**, Left, immunoblots showing YTHDF1–YTHDF3 protein levels in mut*Ythdf1-2-3* and mut*Ythfd2-3* ES cells. PCNA served as loading control. Right, RT–qPCR showing normalized IAP mRNA levels (geometric mean between *Actb* and *Gapdh*) in mutant ES cells relative to wild-type cells using Δ1-, LTR- or *gag*-specific primers. Data are mean ± s.d. from three independent experiments. Immunoblots in **b**, **h** and **i** and the experiment in **d** were repeated at least twice with similar results. Results in **e** and **f** represent averages of two independent CUT&RUN.

degron (AID)[25] to control the depletion of METTL3 and METTL14, individually and in combination (Fig. 4a, Extended Data Fig. 8a, b). The addition of auxin (indole-3-acetic acid (IAA)) resulted in efficient and near-total degradation within 1 h, which persisted over prolonged treatment and was reversible after wash-off (Fig. 4b, Extended Data Fig. 8c). Depletion of METTLs was rapidly followed by substantial and sustainable decrease of m^{6}A RNA methylation levels (Extended Data Fig. 8d). Notably, we observed a progressive, time-dependent accumulation of IAP transcripts after the removal of m^{6}A (Fig. 4c, Extended Data Fig. 8e), whereas levels of cellular proliferation were unaffected (Extended Data Fig. 8f). A similar trend was observed after degron-mediated depletion of ZC3H13 (Extended Data Fig. 8g–j). After 96 h of m^{6}A depletion, levels of IAP mRNA were increased by 7-fold, 5-fold and 15-fold in single METTL3, single METTL14 or METTL3;METTL14 double degron, respectively (Fig. 4c), and this translated into accumulation of IAP-encoded Gag proteins in cytoplasmic speckles (Fig. 4d). Notably, the abundance of IAP mRNA was higher after degron depletion than in established knockouts for individual *Mettl* genes (only twofold increase in *Mettl3* or *Mettl14* knockouts) (Fig. 2b), which suggests the implementation of adaptive mechanisms after prolonged m^{6}A loss. Moreover, the relative upregulation after simultaneous METTL3 and METTL14 degron-mediated depletion compared to single degrons

of METTL3 and METTL14 highlight their functional synergy in reducing IAP mRNA levels. Finally, re-stabilizing the m^{6}A methyltransferase complex after auxin removal resulted in a rapid decline in IAP mRNAs (Fig. 4c, Extended Data Fig. 8e, j). Together, these results suggest that m^{6}A RNA methylation dynamically restrains the cellular availability of IAP mRNAs.

Increased abundance of IAP mRNA may result from transcriptional and/or post-transcriptional effects of the m^{6}A loss. Notably, m^{6}A RNA methylation has been shown to affect chromatin-based regulation of transcription[19,26]. We performed CUT&RUN (cleavage under targets and release using nuclease) experiments to profile permissive (H3K4me3 and H3K27ac) and repressive (H3K9me3) histone marks after 96 h of auxin treatment or dimethylsulfoxide (DMSO) control in METTL3;METTL14 double degron ES cells (AID-METTL3;METTL14). On a global scale, the rapid m^{6}A removal did not alter the coverage of these histone marks on m^{6}A target genes or on different retrotransposon families (Extended Data Fig. 9a–d). When focusing on full-length IAPEz annotations, we observed moderate H3K4me3 gain (Fig. 4e, f), which may contribute to the mRNA upregulation observed after AID-METTL3;METTL14 double degron depletion, although this was not accompanied by a decrease in H3K9me3 or an increase in H3K27ac (Fig. 4e, f). We therefore concluded that acute withdrawal of m^{6}A does not strongly modify chromatin-based regulation of ERVKs in the short term.

Owing to its major effect on genic mRNA lifetime[20], we sought to determine whether m^{6}A could destabilize IAP-derived mRNAs. We used METTL3;METTL14 double degron ES cells to monitor IAP RNA levels after the inhibition of transcription with actinomycin D, and then calculated the half-life rate. IAP mRNA levels and half-life rates were substantially higher after degradation of the m^{6}A methyltransferase complex than in cells treated with DMSO control (Fig. 4g). Importantly, the rapid reintroduction of m^{6}A methylation (by auxin wash-off) restored IAP mRNA degradation (Fig. 4g). The fate of m^{6}A-modified mRNAs is determined by a set of readers, among which the YTH-domain containing proteins YTHDF1, YTHDF2 and YTHDF3 have key roles by directing them to cytosolic compartments where they undergo destabilization and decay[5]. Using RNA immunoprecipitation (RIP), we found that YTHDF2 binds to IAP and MMERVK10C mRNAs (Extended Data Fig. 10a–c), and notably, this occurred in an m^{6}A-dependent manner (Fig. 4h). Finally, we reasoned that, similarly to depleting the m^{6}A writing complex, depleting YTHDF m^{6}A readers should increase IAP mRNA abundance. To account for potential redundancy[27,28], we derived two mutant ES cell lines that exhibited loss of all three YTHDF proteins (Fig. 4i, left, Extended Data Fig. 10d). Depletion of YTHDFs resulted in increased IAP mRNA levels (Fig. 4i, right), which supports the idea that the m^{6}A methylation pathway regulates IAP mRNAs in a post-transcriptional and YTHDF-dependent manner, although other mechanisms may also apply.

Our results provide evidence that m^{6}A RNA methylation directly affects ERV mRNA abundance by accelerating their clearance. This mechanism appears specific to IAP-related ERVK elements, whereas other retrotransposon types may undergo alternative directions and modes of m^{6}A-dependent regulation. Considering the abundance and deleterious effect of ERVKs, this pathway may be particularly relevant in situations of relaxation of chromatin-based control, such as in early mammalian embryos—from which ES cells are derived—or during ageing. The link with YTHDF readers indicates that ERV mRNA decay may occur through phase-partitioning into cytoplasmic processing bodies (P-bodies)[29], consistent with previous observations that IAP mRNAs localize to these structures[30]. In addition, this pathway may cooperatively prevent m^{6}A-modified ERV mRNAs from being reverse transcribed, translated or assembled into protective retrotransposition complexes, providing several layers of control. Notably, m^{6}A mostly occurs on the 5′ UTR of ERVKs, a region that contains the tRNA primer-binding site that is essential for reverse transcription. Finally, m^{6}A-dependent regulation could also dampen the immunogenic potential of ERV-derived RNA species and their ability to trigger inflammatory responses, as seen in human neurodegenerative diseases[3].

Online content

Any methods, additional references, Nature Research reporting summaries, source data, extended data, supplementary information, acknowledgements, peer review information; details of author contributions and competing interests; and statements of data and code availability are available at https://doi.org/10.1038/s41586-020-03135-1.

1. Johnson, W. E. Origins and evolutionary consequences of ancient endogenous retroviruses. *Nat. Rev. Microbiol.* **17**, 355–370 (2019).
2. Barau, J. et al. The DNA methyltransferase DNMT3C protects male germ cells from transposon activity. *Science* **354**, 909–912 (2016).
3. Tam, O. H., Ostrow, L. W. & Gale Hammell, M. Diseases of the nERVous system: retrotransposon activity in neurodegenerative disease. *Mob. DNA* **10**, 32 (2019).
4. Shi, H., Wei, J. & He, C. Where, when, and how: context-dependent functions of RNA methylation writers, readers, and erasers. *Mol. Cell* **74**, 640–650 (2019).
5. Patil, D. P., Pickering, B. F. & Jaffrey, S. R. Reading m^{6}A in the transcriptome: m^{6}A-binding proteins. *Trends Cell Biol.* **28**, 113–127 (2018).
6. Goodier, J. L. & Kazazian, H. H., Jr. Retrotransposons revisited: the restraint and rehabilitation of parasites. *Cell* **135**, 23–35 (2008).
7. Gagnier, L., Belancio, V. P. & Mager, D. L. Mouse germ line mutations due to retrotransposon insertions. *Mob. DNA* **10**, 15 (2019).
8. Hancks, D. C. & Kazazian, H. H. Jr. Roles for retrotransposon insertions in human disease. *Mob. DNA* **7**, 9 (2016).
9. Zamudio, N. & Bourc'his, D. Transposable elements in the mammalian germline: a comfortable niche or a deadly trap? *Heredity* **105**, 92–104 (2010).
10. Rowe, H. M. et al. KAP1 controls endogenous retroviruses in embryonic stem cells. *Nature* **463**, 237–240 (2010).
11. Li, W. et al. MAGeCK enables robust identification of essential genes from genome-scale CRISPR/Cas9 knockout screens. *Genome Biol.* **15**, 554 (2014).
12. Fukuda, K., Okuda, A., Yusa, K. & Shinkai, Y. A CRISPR knockout screen identifies SETDB1-target retroelement silencing factors in embryonic stem cells. *Genome Res.* **28**, 846–858 (2018).
13. Liu, X. et al. UHRF1 targets DNMT1 for DNA methylation through cooperative binding of hemi-methylated DNA and methylated H3K9. *Nat. Commun.* **4**, 1563 (2013).
14. Sadic, D. et al. Atrx promotes heterochromatin formation at retrotransposons. *EMBO Rep.* **16**, 836–850 (2015).
15. Maksakova, I. A. et al. H3K9me3-binding proteins are dispensable for SETDB1/H3K9me3-dependent retroviral silencing. *Epigenetics Chromatin* **4**, 12 (2011).
16. Wen, J. et al. Zc3h13 regulates nuclear RNA m6A methylation and mouse embryonic stem cell self-renewal. *Mol. Cell* **69**, 1028–1038.e6 (2018).
17. Ping, X. L. et al. Mammalian WTAP is a regulatory subunit of the RNA N6-methyladenosine methyltransferase. *Cell Res.* **24**, 177–189 (2014).
18. Greenberg, M. V. C. & Bourc'his, D. Cultural relativism: maintenance of genomic imprints in pluripotent stem cell culture systems. *Curr. Opin. Genet. Dev.* **31**, 42–49 (2015).
19. Liu, J. et al. N^6-methyladenosine of chromosome-associated regulatory RNA regulates chromatin state and transcription. *Science* **367**, 580–586 (2020).
20. Geula, S. et al. m6A mRNA methylation facilitates resolution of naïve pluripotency toward differentiation. *Science* **347**, 1002–1006 (2015).
21. Dominissini, D. et al. Topology of the human and mouse m^{6}A RNA methylomes revealed by m^{6}A-seq. *Nature* **485**, 201–206 (2012).
22. Batista, P. J. et al. m^{6}A RNA modification controls cell fate transition in mammalian embryonic stem cells. *Cell Stem Cell* **15**, 707–719 (2014).
23. Meyer, K. D. et al. Comprehensive analysis of mRNA methylation reveals enrichment in 3′ UTRs and near stop codons. *Cell* **149**, 1635–1646 (2012).
24. Abakir, A. et al. N^6-methyladenosine regulates the stability of RNA:DNA hybrids in human cells. *Nat. Genet.* **52**, 48–55 (2020).
25. Nishimura, K., Fukagawa, T., Takisawa, H., Kakimoto, T. & Kanemaki, M. An auxin-based degron system for the rapid depletion of proteins in nonplant cells. *Nat. Methods* **6**, 917–922 (2009).
26. Li, Y. et al. N^6-Methyladenosine co-transcriptionally directs the demethylation of histone H3K9me2. *Nat. Genet.* **52**, 870–877 (2020).
27. Zaccara, S. & Jaffrey, S. R. A unified model for the function of YTHDF proteins in regulating m^{6}A-modified mRNA. *Cell* **181**, 1582–1595.e18 (2020).
28. Lasman, L. et al. Context-dependent functional compensation between Ythdf m^{6}A reader proteins. *Genes Dev.* **34**, 1373–1391 (2020).
29. Ries, R. J. et al. m^{6}A enhances the phase separation potential of mRNA. *Nature* **571**, 424–428 (2019).
30. Lu, C., Contreras, X. & Peterlin, B. M. P. P bodies inhibit retrotransposition of endogenous intracisternal A particles. *J. Virol.* **85**, 6244–6251 (2011).

Methods

Data reporting and statistical analysis

No statistical methods were used to predetermine sample size. The experiments were not randomized and the investigators were not blinded to allocation during experiments and outcome assessment. All statistical tests, resulting *P* values and observation numbers are indicated in the figure panels or legends.

Data visualization

Unless stated otherwise, heat maps, violin plots, box plots, Venn diagrams, density plots, dot plots and bar plots that visualize deep-sequencing analyses were generated using ggplot2. Box plots always show the median as the centre line, box limits correspond to upper and lower quartiles, and whiskers cover 1.5× the interquartile range. Volcano plots visualizing retrotransposon expression changes from RNA-seq and bar graphs visualizing ELISA and RT–qPCR experiments were generated using Prism 8.3.0. Dot plots and histogram visualizing FACS analyses were generated using NovoExpress software (v.1.2.1).

Cell culture

Mouse embryonic day (E) 14 ES cells were grown in two different media: serum + LIF consisted in Glasgow medium (Sigma), 15% FBS (Gibco), 2 mM L-glutamine, 0.1 mM MEM non-essential amino acids (Gibco), 1 mM sodium pyruvate (Gibco), 0.1 mM β-mercaptoethanol, 1,000 U ml^{-1} leukaemia inhibitory factor (LIF, Miltenyi Biotec); 2i + LIF was made of 50% Neurobasal medium (Gibco), 50% DMEM/F12 (Gibco), 2 mM L-glutamine (Gibco), 0.1 mM β-mercaptoethanol, Ndiff Neuro-2 medium supplement (Millipore), B-27 medium supplement (Gibco), 1,000 U ml^{-1} LIF, 3 μM GSK3 inhibitor (CT-99021), 1 μM MEK inhibitor (PD0325901). Cells were cultured in 0.2% gelatin-coated flasks at 37 °C with 5% CO_2. Except for the CRISPR–Cas9 loss-of-function screens that were performed in serum + LIF medium, all experiments were performed in 2i + LIF medium. Mycoplasma-free status of the cell cultures was verified.

Plasmid construction

IAPEz reporter. Plasmids used to target *ROSA26* (pEN111) and *TIGRE* (also known as *Igs7*) (Addgene 92141) loci, and the *ROSA26*- and *TIGRE*-specific sgRNA-encoding plasmids (Addgene 86234 and 92144, respectively) were provided by E. Nora (UCSF). The IAPEz-5′LTR-5′UTR-gag(3-60nt) consensus sequence was obtained from RepeatMasker and/or from repbase (http://www.repeatmasker.org/) synthetized and cloned into pUC57 by GenScript (Supplementary Table 1). To make the IAPEz reporter (pTCH1), IAPEz-5′LTR-5′UTR-gag(3-60nt) sequence and the GFP-T2A-blasticidin resistance cassette (hereafter denoted as BlastR) were combined using extension PCR and inserted it into the pEN111 backbone using the ClaI site. To insert the *Cas9* gene at the *TIGRE* locus, 3× Flag-NLS-Cas9 was PCR amplified from pX459 expression vector (Addgene 62988) and inserted into plasmid 92141 backbone using BamHI and XhoI sites (pTCH2).

Plasmids for N terminus tagging with AID domain for auxin-inducible degron. The plasmids to target OsTIR1 at the *TIGRE* locus (Addgene 92141) and the *TIGRE*-specific sgRNA-encoding plasmid (see above) were provided by E. Nora (UCSF). The plasmids to target AID inserts into the gene-of-interest N terminus were generated as follows: either puromycin resistance (PuroR)-P2A-3×Flag-AID, or BlastR-P2A-3×Flag-AID inserts were cloned into pUC19 backbone (pFD71 with puromycin resistance gene and pFD75 with blasticidin S-resistance gene). Next, homology arms ranging from 320 to 530 bp depending on the gene (flanking both sides, but excluding ATG start codon) for *Mettl3*, *Mettl14* and *Zc3h13* were PCR amplified from mouse genomic DNA and inserted into pFD71 or pFD75 surrounding and in frame with AID insert using EcoRI/NcoI sites for upstream homology arms and AgeI/HindII for downstream homology arms. Final expression vectors were used as follows: pTCH3 (BlastR-P2A-3×Flag-AID-METTL3_Nter), pTCH4 (BlastR-P2A-3×Flag-AID-METTL4_Nter) and pFD119 (BlastR-P2A-3×Flag-AID-ZC3H13_Nter) to generate individual endogenous degron ES cell lines for aforementioned genes. The pTCH4 and pTCH5 (PuroR-P2A-3×Flag-AID-Mettl3) were used sequentially to generate the AID-METTL3;-METTL14 double degron ES cell line. For the sgRNA cloning, the pX459 plasmid (Addgene 62988) was digested with BbsI immediately downstream of the U6 promoter and annealed DNA duplex corresponding to the target sgRNA sequences were ligated. sgRNA sequences were chosen to overlap with the gene TSS, so that after introduction of the AID the sgRNA-specific sequences were disrupted. sgRNA sequences used for degron targeting are listed in Supplementary Table 2.

Cell transfection and clone isolation

All transgenic insertions and mutations were performed using Amaxa 4D nucleofector (Lonza). For each nucleofection, 3×10^6–5×10^6 cells were electroporated with 1–3 μg of nonlinearized targeting vector and/or sgRNA/Cas9-encoding plasmids and plated at a low density. Two days later, cells were selected with puromycin (1 μg ml^{-1}, Life Technologies) or blasticidin S (5 μg m^{-1}) for 2 and 5 days, respectively, and individual clones were picked and screened by PCR. Flippase-mediated removal of puromycin-resistance cassettes were performed for the IAPEz reporter cell line (from both *ROSA26* and *TIGRE* loci) and for puromycin resistance cassette for AID-METTL3;METTL14 double degron from the *TIGRE* locus. For the IAPEz reporter cell line, functionality of the reporter cassette was confirmed by doxycycline (dox) induction followed by FACS and fluorescence microscopy analyses while Cas9 expression and activity was confirmed by *Kap1*-specific sgRNA introduction (see below) and western blot analysis. To generate *Mettl3*, *Mettl14*, *Wtap*, *Zc3h13*, *Ythdf2* and combined *Ythdf* mutant ES cells, two sgRNAs for each gene were designed using the online CRISPOR Design Tool[31] to introduce indels and/or deletions. For sgRNA cloning, the pX459 plasmid (Addgene 62988) was digested with BbsI immediately downstream of the U6 promoter and annealed DNA duplex corresponding to the target sgRNA sequences were ligated. The *Mettl3*-knockout cells were created by deleting part of exon 4; *Mettl14*-knockout by deleting part of exon 1; *Zc3h13*-knockout by deleting part of exon 9; and sgRNA targeting of *Wtap* gene resulted in single nucleotide insertion and premature stop codon in exon 4. *Ythdf2*-knockout cells were generated by deleting part of exon 4. The mut*Ythdf1-2-3* and mut*Ythd2-3* ES cells were obtained by simultaneous introduction of six sgRNAs targeting the *Ythdf1*, *Ythdf2* and *Ythdf3* genes. Protein loss was confirmed by western blot for all mutant cell lines; in addition, m^6A ELISA assays was carried out for *Mettl3*-, *Mettl14*-, *Wtap*- and *Zc3h13*-knockout lines. For degron lines, proper insertion and AID-fusion protein activities were confirmed by genotyping, western blot analysis and m^6A ELISA. For sgRNA sequences used for generation of knockout, mutant and degron lines see Supplementary Table 2.

Cell treatments

IAPEz reporter expression was induced after the administration of doxycycline (1 μg ml^{-1}). Auxin-mediated depletion of target proteins was achieved by supplementing culture medium with auxin (Sigma) at the recommended concentration of 500 μM. Auxin-containing medium was renewed every 24 h. For auxin wash-off, auxin-containing medium was removed, cells were rinsed twice with PBS, and exposed to auxin-free medium. Blockade of transcription with actinomycin D was achieved by supplementing culture medium with 5 μg ml^{-1} actinomycin D (Sigma) .

Lentivirus production and lentiviral-based *Kap1*-specific sgRNA knockout

Two previously described sgRNAs specific to the *Kap1* gene[32] (Supplementary Table 2) were incorporated into plentiGuide-puro vector

(Addgene 52963). For production of lentiviral particles, HEK293FT cells were co-transfected with 3.33 µg of either of the Kap1 lentiGuide-puro constructs, 2.5 µg psPAX2 packaging plasmid and 1 µg pMD2.G envelope plasmid using Lipofectamine 2000 (Invitrogen). Lentiviral supernatant was collected, filtered with 0.45-µm filter, concentrated using Amicon Ultra centrifugal filter (Millipore, 100-kDa cut-off) and added to pre-plated IAPEz reporter cells supplemented with 8 µg ml^{-1} polybrene (Millipore). Twelve hours after infection, the medium was replaced and supplemented with puromycin (1 µg ml^{-1}). After 48 h of puromycin selection the medium was replaced and supplemented with blasticidin S (5 µg ml^{-1}) for additional 72 h.

Protein extraction and western blotting

Cells were trypsinized, washed once in medium and once in PBS and pelleted for 5 min at 1,000 rpm. Cell pellets were resuspended in RIPA buffer (1× PBS, 0.5% sodium deoxycholate, 0.1% SDS, 1% Igepal CA-630) containing protease inhibitors (Roche) and incubated on ice for 20 min. Lysates were then centrifuged for 20 min at 16,400 rpm, at 4 °C and supernatants were kept. Protein concentration was determined using Bradford assay and protein extracts were boiled for 10 min in LDS buffer (Life Technologies) containing 200 mM DTT. Equal amounts of protein were loaded on 4–12% Bis-Tris gel (NuPAGE), or 3–8% Tris-Acetate gel (NuPAGE) for ZC3H13 detection. Transfer was performed on a 0.45-µm nitrocellulose membrane (GE Healthcare) using wet-transfer system, blocked with 5% milk in PBS (+Igepal CA-630 to a final concentration of 0.3%) for 1 h at room temperature. Membranes were incubated with primary antibodies (Supplementary Table 3) at 4 °C overnight in 1% milk in PBS (supplemented with 0.3% Igepal CA-630), washed five times with PBS supplemented with 0.3% Igepal CA-630 and incubated with HRP-conjugated secondary antibodies for 1 h at room temperature and washed again five times. Signal was detected using LumiLight Plus Kit (Roche) on the Chemidoc MP imaging system (BioRad). For uncropped images of western blot membranes, see Supplementary Fig. 1.

FACS analysis

Cells were collected, washed with PBS to remove residual medium and proceeded to analyse GFP expression using NovoCyte 2000R (ACEA Biosciences) flow cytometer and NovoExpress software (v1.2.1). The percentage of GFP-positive cells was determined upon definition of three gates: (i) FSC-H *vs* SSC-H to isolate cells from debris, (ii) SSC-H versus SSC-A to isolate single cells and (iii) SSC-H versus FITC-H for detection of GFP-positive population. For pseudocolour plots and gating strategy see Supplementary Fig. 2.

Genome-wide screen in IAPEz reporter mouse ES cells (screens I and II)

Approximately 300 × 10^6 IAPEz reporter ES cells expressing Cas9 were lentivirally infected with a genome-wide Mouse Two Plasmid Activity-Optimized CRISPR Knockout Library (Addgene 1000000096) as described above, containing 188,509 sgRNAs targeting 18,986 genes and 199 intergenic sgRNAs at a multiplicity of infection of 0.2–0.3 (measured by puromycin-resistance gene co-delivered with the lentiviral vector) and selected for lentiviral integration using puromycin (1 µg ml^{-1}) for 3 days. In screen I, the culture was expanded for another 4–8 days. On days 4, 6 and 8 of expansion, 200 × 10^6 cells were split into blasticidin S-selecting conditions (for 9, 7 and 5 days, respectively) and non-selection conditions (9 days). Cells in non-selection conditions were maintained at minimum level of 100 × 10^6 cells and logarithmic growth. After 9 days, 3 × 10^6–5 × 10^6 cells from selection conditions and 100 × 10^6 non-selection conditions were washed three times with PBS and pelleted by centrifugation for genomic DNA extraction using GeneElute Mammalian Genomic DNA Miniprep kit (Sigma) and Quick-DNA Midiprep Plus kit (Zymo Research), respectively, following the manufacturers guidelines. The sgRNA-encoding insertions were PCR-amplified using Agilent Herculase II Fusion DNA Polymerase (600675). These libraries were then sequenced using Illumina HiSeq 2500 (approximately 5 million–10 million reads with sgRNA sequence per condition; around 40× coverage per library element in non-selection conditions, screen I). As screen I demonstrated that longer blasticidin S treatment resulted in better intergenic sgRNA depletion, we performed screen II in two biological replicates with 9-day-long blasticidin S selection after either 8-day-long or 17-day-long cell culture (early and late selection, respectively). After genomic DNA extraction and library amplification, libraries were sequenced using Illumina HiSeq 2500 (SE65) (approximately 30 million–35 million reads per condition; around 170× coverage per library element in early and late non-selection conditions, screen II. See Supplementary Table 1 for the primer sequences used to amplify the libraries.

Immunofluorescence

Cells were plated on fibronectin-coated (Sigma) glass coverslips. For IAPEz-GFP reporter reactivation control, doxycycline (1 µg ml^{-1}) was added for 24 h. The next day, cells were fixed with 3% paraformaldehyde for 10 min at room temperature, rinsed three times with PBS, incubated 3 min in 0.3 µg ml^{-1} DAPI and rinsed again with PBS. For detection of IAP-GAG, after fixation, cells were permeabilized for 4 min with PBS/0.5× Triton X-100 on ice, blocked with 1% BSA/PBS for 15 min, incubated for 40 min with rabbit anti-mouse IAP-GAG antibody (gift from B. Cullen), 40 min with secondary antibodies and 3 min in 0.3 µg ml^{-1} DAPI at room temperature. Slides were mounted with VECTASHIELD medium (Vector Laboratories). Images were obtained with an Upright Spinning disk Confocal Microscope (Roper/Zeiss) and processed with Image J.

RT–qPCR analysis

Total RNA was extracted using Trizol (Life Technologies). Genomic DNA was removed by DNase I treatment (Qiagen), precipitated and resuspended in DNase/RNase-free water. Next, 10 µg of RNA was used for a second round of purification using RNeazy Mini columns (Qiagen) and 500 ng RNA was reverse-transcribed using random priming with Superscript III (Life Technologies). Quantitative PCR was performed using the SYBR Green Master Mix on the Viia7 thermal cycling system (Applied Biosystem). Relative expression levels were normalized to *Gapdh* or *Actb* (indicated in respective figures) using the $\Delta\Delta C_t$ method. For primer sequences, see Supplementary Table 1.

RNA stability assay

For RNA stability assay, 0.5 × 10^6 AID-METTL3;METTL14 dd ES cells treated with either 500 µM auxin or DMSO for 96 h or after 48-h auxin wash-off were re-plated on fibronectin-coated 6-cm plates 24 h before addition of actinomycin D. Next, medium were renewed and supplemented with 5 µg ml^{-1} actinomycin D (Sigma) to inhibit transcription. Total RNA was extracted at indicated time points and used for RT–qPCR. The half-life of IAPΔ1 was calculated according to the following equation: $\ln(C_i/C_0) = -kt_i$, in which k is the degradation rate, C_i is the mRNA value at time i, and t_i is the time interval in hours[33]. First, we calculated degradation rate k_i from each time point. The half-life $t_{1/2}$ is $\ln(2)/k_a$, in which k_a is the average degradation rate measured across the different time points.

m^{6}A ELISA

m^{6}A ELISA was performed using an m^{6}A RNA methylation colorimetric assay kit (Abcam, ab185912) according to manufacturer's protocol, and using 200 ng of RNA. After incubation in the last developer solution, the reaction was stopped by adding 100 µl of STOP solution at the moment positive control wells turned medium blue. It is crucial to continuously control the progressive colour change for the positive control; prolonged incubation will result in signal saturation in the experimental wells and potential masking of differences between tested conditions. Absorbance was measured at 450 nm within 5 min using absorbance microplate reader.

RNA immunoprecipitation

For each replicate, 1.5×10^7 cells were collected, washed with ice-cold PBS, resuspended in 1 ml of RIP lysis buffer (50 mM Tris-HCl pH 7.4, 150 mM NaCl, 1 mM EDTA, 1 mM DTT, 0.5% Igepal CA-630, containing 40 U ml^{-1} of RNasin and protease inhibitors (Roche)). Lysates were placed on ice for 20 min and centrifuged at 4 °C to remove cell debris. Supernatants containing RNA–protein complexes were collected and 50 µl was kept for input control. Remaining lysates were precleared with M-280 sheep anti-rabbit IgG magnetic beads (Thermo Fisher Scientific) and incubated with either 5 µg of YTHDF2 antibody or rabbit IgG rotating overnight at 4 °C. Next, 25 µl of beads was added and samples were rotated for additional 2 h at 4 °C. Beads were washed with RIP lysis buffer five times for 10 min and RNA was isolated from the beads as well as input samples using Trizol. Genomic DNA was removed by DNase I treatment (Qiagen), precipitated and resuspended in DNase/RNase-free water. Next, purified RNA underwent a second round of purification using RNeazy Mini columns (Qiagen). Immunoprecipitated and input RNAs were reverse transcribed using random priming with Superscript III (Life Technologies). Reverse transcription and real-time quantitative PCR were used to measure abundance.

Poly-A RNA sequencing

Total RNA was extracted using Trizol (Life Technologies). Genomic DNA was removed by in solution DNaseI treatment (Qiagen), RNA was precipitated and resuspended in DNase/RNase-free water. Next, 10 µg of RNA was used for a second round of purification using RNeazy Mini columns (Qiagen). RNA integrity was evaluated on TapeStation 4200 (Agilent) using RNA ScreenTape (5067-5576), requiring a minimal integrity number (RIN) of 9. Libraries were prepared according to Illumina's instructions accompanying the TruSeq Stranded mRNA Library Prep Kit. Approximately 800 ng of RNA per replicate was used for library preparation. After library preparation, the length profiles were assessed with the LabChip GX Touch HT system (Perkin Elmer) and equimolar pool from all samples was prepared. Molarity of the pool was quantified by qPCR using KAPA Library Quantification Kit and the CFX96 qPCR system (Biorad) before sequencing. Samples were sequenced using Novaseq 6000 (PE100, approximately 90 million clusters per replicate).

MeRIP-seq

MeRIP-seq was carried out using Magna MeRIP m^6A Kit (Millipore) according to the manufacturer's instructions. In short, total RNA was extracted using Trizol (Life Technologies). DNaseI-treated RNA samples were chemically fragmented into 100-nucleotide-long fragments and 350 µg of total RNA were subjected to each immunoprecipitation with affinity purified anti-m^6A antibody in presence of RNase inhibitor. Bound m^6A-methylated RNA fragments were eluted with free N6-methyladenosine, purified using RNeazy Kit (Qiagen) and processed for library generation using SMARTer Stranded Total RNA-Seq Kit v2 - Pico Input Mammalian (TaKaRa) following the manufacturer's recommendations, but without fragmentation step (9 ng of RNA per replicate). Sequencing was performed using Illumina Novaseq 6000 (PE100, approximately 50 million to 90 million clusters per replicate). The m^6A IP for wild-type and *Mettl3*-knockout cells was performed independently three times. Input for each cell line was sequenced as a control.

CUT&RUN

For chromatin profiling, we performed CUT&RUN[34] on AID-METTL3;METTL14 double degron cells treated with either DMSO (control) or auxin for 96 h in two biological replicates. In brief, 2×10^5 cells were washed with PBS, three times with wash buffer (20 mM HEPES-KOH pH 7.9, 150 mM NaCl, 0.5 mM spermidine and Protease Inhibitors (Roche)) at room temperature, then resuspended in 1 ml of washing buffer. Next, 10 µl of concanavalin A-coated magnetic beads (Bangs Laboratories, BP531), pre-washed and resuspended in binding buffer (20 mM HEPES-KOH, pH 7.9, 10 mM KCl, 1mM $CaCl_2$, 1 mM $MnCl_2$), were added to the cells. After 10 min incubation at room temperature under rotation, bead-bound cells were isolated on a magnetic stand and resuspended in 400 µl of antibody buffer (wash buffer supplemented with 0.02% digitonin (Millipore, 300410) and 2 mM EDTA) containing 2 µg of anti-H3K4me3, -H3K27ac or -H3K9me3 antibody or 2 µg of rabbit IgG (Supplementary Table 3). After 15 min incubation at room temperature under rotation, cells were washed three times in 1 ml of digitonin(dig)-wash buffer (wash buffer supplemented 0.02% digitonin), incubated with pA-MNase (400 µl of dig-wash buffer containing 700 ng ml^{-1} pA-MNase, produced by the Protein Core Facility of Institut Curie) and washed again three times in 1 ml of dig-wash buffer. Cells were then resuspended in 150 µl of dig-wash buffer, transferred to 1.5 ml tubes, and equilibrated to 0 °C in a metal block for 10 min on ice. To initiate pA-MNase-dependent digestion, $CaCl_2$ was added to a final 2 mM concentration, incubation was carried out at 0 °C for 30 min, and stopped by adding 150 µl of 2 × STOP solution (200 mM NaCl, 20 mM EDTA, 5 mM EGTA, 0.1% Igepal CA-630, 40 µg ml^{-1} glycogen). RNase A was added to a final concentration of 50 µg ml^{-1} and samples were incubated at 37 °C for 20 min. Samples were placed on a magnetic stand, supernatant was transferred to low-binding tubes and SDS and proteinase K were then added to final concentrations of 0.1% and 300 µg ml^{-1}, respectively, and samples were incubated at 70 °C for 30 min. Total DNA was extracted by phenol/chloroform followed by two rounds of ethanol precipitation, eluted in 40 µl of 1 mM Tris-HCl pH 8.0 and 0.1 mM EDTA, and quantified and analysed using Qubit and TapeStation assays. CUT&RUN libraries were prepared using the Accel-NGS 2S Plus DNA Library Kit (Swift Biosciences) according to the manufacturer's protocol. Samples were sequenced using NovaSeq 6000 (PE50, approximately 60 million clusters per replicate).

Genome-wide CRISPR–Cas9 screen analysis

The sequenced reads were mapped to the sgRNA library. Only reads that contained one sgRNA sequence without mismatch were counted. The MAGeCK[11] test command line (version 0.5.8) was used to rank sgRNAs and genes with following parameters: –norm-method total–adjust-method fdr–remove-zero-threshold 10–gene-lfc-method alphamean–remove-zero both. For screen II, the sequencing primer was oriented in the opposite direction to the sgRNA, therefore the CRISPR mouse pooled library was reverse-complemented before counting.

RNA-seq analysis

Adapters were trimmed using Atropos v.1.1.16[35]. Paired-end read alignment was performed onto the Mouse reference genome (mm10) with STAR v.2.7.0a[36] reporting randomly one position, allowing 6% of mismatches (–outFilterMultimapNmax 5000–outSAMmultNmax 1–outFilterMismatchNmax 999–outFilterMismatchNoverLmax 0.06). Repeat annotation was downloaded from RepeatMasker (http://www.repeatmasker.org/). To reconstruct full-length LTR copies, we used the same strategy as done previously[10] using the perl tool 'one code to find them all'[37]. Reconstructed transposons annotation and basic genes annotation from GENCODE v.18 were merged and used as input for quantification with FeatureCounts v1.5.1[38]. Differential expression analysis was performed using edgeR's normalization combined with voom transformation from limma R package[39,40]. *P* values were computed using limma and adjusted with the Benjamini–Hochberg correction. Genes and transposon families were declared as differentially expressed if FDR < 5% and $\log_2$FC > 0.75. Upregulated genes in all four knockout lines were annotated with proximal retrotransposon elements (overlap with promoter regions defined as −5 kb to +1 kb from the TSS). Randomized gene sets were created 100 times and were annotated to proximal retrotransposon elements to compute permutation test using regioneR[41] R package.

Transposon element-based analysis was performed using only uniquely mapped reads by retrieving reads with NH tag equal to 1. To avoid confounding effects between expression from retrotransposon copies and from genes, elements overlapping genes in the same direction were removed from RepeatMasker annotations. FeatureCounts v.1.5.1 was used for the quantification and only copies with at least 10 reads in at least one sample were conserved. RRACH motifs were searched into the 5′ UTR sequences of individual IAP copies using RSAT dna pattern. Division into three categories of RRACH motif number (7–8, 9–10 and 11–18) was performed to homogenize the number of IAP copies per category.

To estimate intron retention between genes and single IAP copies, reads alignment was performed using specific parameters to report only uniquely mapped reads with STAR v.2.7.0a[36] (–outFilterMultimapNmax 1–outSAMmultNmax 1). Unannotated splice junctions detected by STAR was annotated with GENCODE v.18 and IAP LTR elements from RepeatMasker annotation to retrieve splicing events between a gene and an IAP element. The number of uniquely mapped reads crossing the splicing events was calculated for each sample and normalized by the library size.

MeRIP-seq analysis

Due to the addition of 3 nucleotides on 5′-end of the second sequencing read (R2) from the Pico v.2 SMART Adaptor, paired-end reads were trimmed using Trim Galore v.0.4.4 with the options: –three_prime_clip_R1 3–clip_R2 3 (http://www.bioinformatics.babraham.ac.uk/projects/trim_galore/). Reads were aligned onto the mouse ribosomal sequence (GenBank: BK000964.3) using Bowtie v.1.2 allowing at most three mismatches[42]. Previously unmapped reads were aligned onto the mouse reference genome (mm10) using STAR v.2.6.0c reporting randomly one position, allowing 4% of mismatches (–outFilterMultimapNmax 5000–outSAMmultNmax 1–outFilterMismatchNmax 999–outFilterMismatchNoverLmax 0.04). PCR duplicates were removed using STAR with the option –bamRemoveDuplicatesType UniqueIdenticalNotMulti. Bigwig files were produced with deepTools v.2.5.3[43] using the option –normalizeUsingRPKM. Peaks enriched in the MeRIP sample over the input control were defined using MACS2 peak-caller[44] with a genome size of 994,080,837 bp[20] and the FDR threshold of 5%. Reads were extended to 200-bp-long fragments. Only peaks called in at least two replicates were used for downstream analysis. Peaks intensity was calculated using FeatureCounts v.1.5.1[38] and normalized to background (reads not falling into peaks) and to peak length. GENCODE v.18 was used to define 5′UTR, 3′UTR, intronic and exonic regions. Retrotransposon annotations (RepeatMasker) were downloaded from UCSC table browser. Genes overlapping with at least one peak were used to calculate coverage along the genic region (5′UTR, coding sequence and 3′UTR) with trumpet R package[45]. Mapped reads onto the Mouse reference genome overlapping with IAP and L1MdA_I elements were extracted as single-end reads and mapped to the full-length IAP (GenBank: M17551.1) and L1MdA_I consensus sequences with Bowtie2 v.2.2.9[46] with these parameters: –local -N 1. Coverage along the consensus sequence was normalized to background (reads not falling into peaks) as was done previously for peak intensities. Rolling mean was calculated for a window of 50 bp to smooth the signal. RRACH motif was searched into the IAP consensus sequence using RSAT dna pattern. Intragenic peaks in the wild-type condition were used to define m^{6}A-bound genes. In addition, a threshold of 1 RPKM in the input wild-type samples was put to be sure that the gene is expressed. Genes with RPKM higher than 1 and not overlapping with a m^{6}A peak were defined as non-m^{6}A bound genes.

CUT&RUN analysis

Paired-end reads were trimmed using Trim Galore v0.4.4. The alignment was performed onto a concatenated genome using the mouse reference genome (mm10) and the *Escherichia coli* genome (str. K-12 substr. MG1655, GenBank: NC_000913) with STAR v.2.7.0a[36] reporting randomly one position, allowing 6% of mismatches (–outFilterMultimapNmax 5000–outSAMmultNmax 1–outFilterMismatchNmax 999–outFilterMismatchNoverLmax 0.06). PCR duplicates were removed using Picard v.2.6.0 (http://broadinstitute.github.io/picard/). Reconstructed transposon annotation was used as input for quantification with FeatureCounts v.1.5.1[38] using reads mapped onto the mouse genome. Normalization of counts per million was performed using as library size the number of mapped reads onto the mouse genome.

Reporting summary

Further information on research design is available in the Nature Research Reporting Summary linked to this paper.

Data availability

The raw imaging data that support the findings of this study are available from the corresponding authors on request owing to size considerations. All sequencing data derived from CRISPR–Cas9 screens I and II, RNA-seq, MeRIP-seq and CUT&RUN have been deposited in the Gene Expression Omnibus (GEO) under accession number GSE145616. Previously published data were downloaded from GEO: *Mettl3* control and *Mettl3* knockout nuclear RNA-seq: (GSE133585)[19]. Source data are provided with this paper.

31. Haeussler, M. et al. Evaluation of off-target and on-target scoring algorithms and integration into the guide RNA selection tool CRISPOR. *Genome Biol.* **17**, 148 (2016).
32. Walter, M., Teissandier, A., Pérez-Palacios, R. & Bourc'his, D. An epigenetic switch ensures transposon repression upon dynamic loss of DNA methylation in embryonic stem cells. *eLife* **5**, 1–30 (2016).
33. Chen, C. Y. A., Ezzeddine, N. & Shyu, A. B. Messenger RNA half-life measurements in mammalian cells. *Methods Enzymol.* **448**, 335–357 (2008).
34. Skene, P. J. & Henikoff, S. An efficient targeted nuclease strategy for high-resolution mapping of DNA binding sites. *eLife* **6**, 1–35 (2017).
35. Didion, J. P., Martin, M. & Collins, F. S. Atropos: specific, sensitive, and speedy trimming of sequencing reads. *PeerJ* **5**, e3720 (2017).
36. Dobin, A. et al. STAR: ultrafast universal RNA-seq aligner. *Bioinformatics* **29**, 15–21 (2013).
37. Bailly-Bechet, M., Haudry, A. & Lerat, E. 'One code to find them all': a perl tool to conveniently parse RepeatMasker output files. *Mob. DNA* **5**, 1–15 (2014).
38. Liao, Y., Smyth, G. K. & Shi, W. featureCounts: an efficient general purpose program for assigning sequence reads to genomic features. *Bioinformatics* **30**, 923–930 (2014).
39. Robinson, M. D., McCarthy, D. J. & Smyth, G. K. edgeR: a Bioconductor package for differential expression analysis of digital gene expression data. *Bioinformatics* **26**, 139–140 (2010).
40. Ritchie, M. E. et al. limma powers differential expression analyses for RNA-sequencing and microarray studies. *Nucleic Acids Res.* **43**, e47 (2015).
41. Gel, B. et al. regioneR: an R/Bioconductor package for the association analysis of genomic regions based on permutation tests. *Bioinformatics* **32**, 289–291 (2016).
42. Langmead, B., Trapnell, C., Pop, M. & Salzberg, S. L. Ultrafast and memory-efficient alignment of short DNA sequences to the human genome. *Genome Biol.* **10**, R25 (2009).
43. Ramírez, F. et al. deepTools2: a next generation web server for deep-sequencing data analysis. *Nucleic Acids Res.* **44** (W1), W160–W165 (2016).
44. Zhang, Y. et al. Model-based analysis of ChIP-Seq (MACS). *Genome Biol.* **9**, R137 (2008).
45. Zhang, T., Zhang, S. W., Zhang, L. & Meng, J. trumpet: transcriptome-guided quality assessment of m^{6}A-seq data. *BMC Bioinformatics* **19**, 260 (2018).
46. Langmead, B. & Salzberg, S. L. Fast gapped-read alignment with Bowtie 2. *Nat. Methods* **9**, 357–359 (2012).

Acknowledgements We thank the members of the Bourc'his laboratory for their support; M. Greenberg and A. Shkumatava for critical reading of the manuscript; G. Cristofari and J. J. Zylicz for suggestions; I. Pinheiro for help with FACS analysis; E. Nora for targeting plasmids; and M. Schultz and M. Borensztein for assistance with cell culture and immunofluorescence experiments. We acknowledge the ICGex NGS platform of the Institut Curie -supported by grants ANR-10-EQPX-03 (Equipex) and ANR-10-INBS-09-08 (France Génomique) from the Agence Nationale de la Recherche- and the Cell and Tissue Imaging Platform (PICT-IBiSA) of Institut Curie -member of the French National Research Infrastructure France-BioImaging (ANR-10-INBS-04). The laboratory of D.B. is part of the LABEX DEEP (ANR-11-LABX-0044, ANR-10-IDEX-0001-02). This work was supported by the Fondation Bettencourt Schueller, the Association Robert Debré pour la Recherche Médicale (ARDRM), the Fondation pour la Recherche Médicale (FRM) and the Association de Recherche contre le Cancer (ARC-PJA-20191209637). T.C. was a recipient of an EMBO postdoctoral fellowship; E.R. and M.D were supported by PhD fellowships from la Ligue contre le Cancer and from Région Ile-de-France, respectively.

Author contributions D.B. and T.C. conceived and designed the study. T.C. performed the genetic screen, genetic engineering of the different ES cell lines (reporter, genetic knockouts and auxin-degron), RNA-seq, MeRIP-seq, degron experiments, actinomycin D assays, m^{6}A quantification by ELISA and immunoblots. E.R. contributed to generating and characterizing ES cell knockouts of *Mettl3*, *Mettl14*, *Wtap*, *Zc3h13*, *Ythdf1*, *Ythdf2* and *Ythdf3* and aided degron

experiments. T.C., M.D. and L.B. performed CUT&RUN experiments. S.R. and C.F. aided the genetic screen, and M.D. the MeRIP-seq. F.D. provided degron-targeting vectors and helped with degron design. A.T. performed the bioinformatic analyses. S.L. aided sequencing library preparations. D.B. and T.C. interpreted the data and wrote the manuscript. All authors read and approved the final manuscript.

Competing interests The authors declare no competing interests.

Additional information

Supplementary information The online version contains supplementary material available at https://doi.org/10.1038/s41586-020-03135-1.

Correspondence and requests for materials should be addressed to T.C. or D.B.

Peer review information *Nature* thanks Miguel Branco and the other, anonymous, reviewer(s) for their contribution to the peer review of this work. Peer review reports are available.

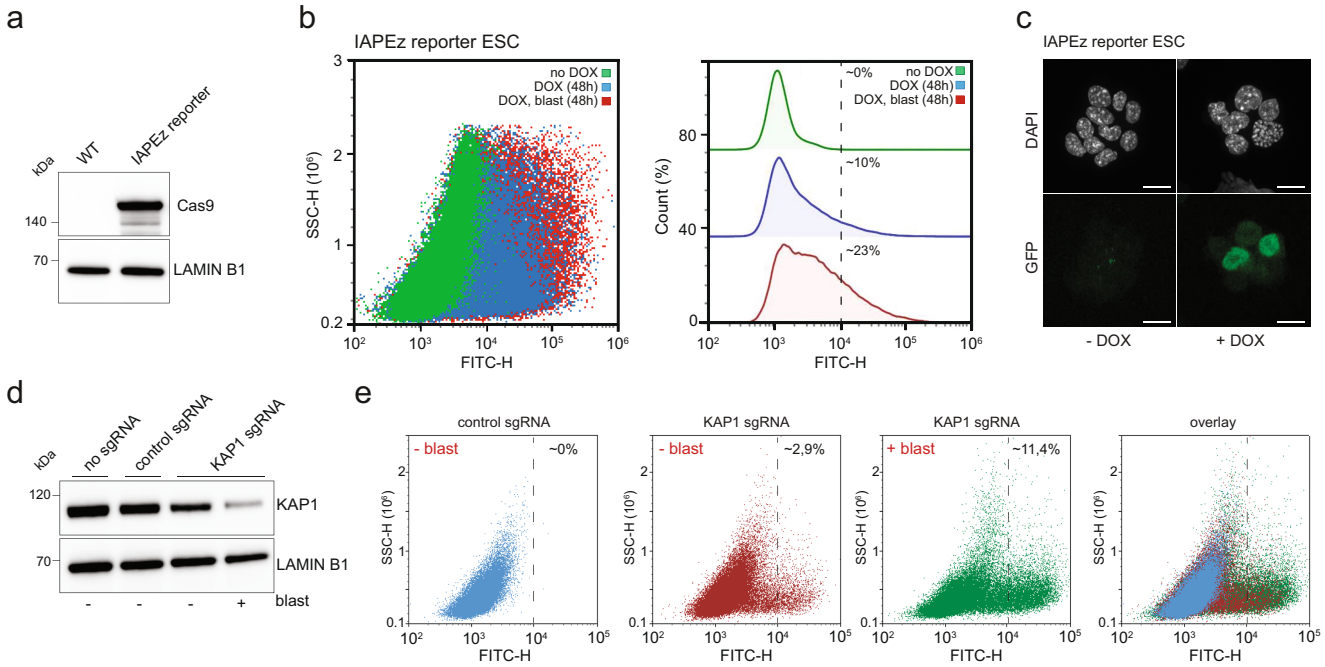

Extended Data Fig. 1 | Validation of the IAPEz-reporter ES cell line. **a**, Immunoblot showing Cas9 protein levels in parental (E14) and doxycycline (dox)-inducible IAPEz-reporter ES cells. Lamin B1 served as loading control. **b**, Flow cytometry analysis of GFP expression in IAPEz-reporter ES cells before and upon 48 h of dox (1 μM) induction and blasticidin (blast, 5 μg ml^{-1}) selection. Left, overlaid dot blots (last 130,000 events) and histograms normalized to 100% scale (right). Analysis was performed using NovoExpress software (Acea Biosciences). For pseudocolour plots and gating strategy, see Supplementary Fig. 2. Note that blasticidin selection further increases the fraction of GFP-positive cells, and not all blasticidin-resistant cells accumulate detectable GFP levels. Therefore, blasticidin selection is more sensitive than the GFP signal to subtle changes in the expression of IAPEz reporter. **c**, Immunofluorescence detection of GFP in dox-induced IAPEz-reporter ES cells. Scale bar, 10 μm. **d**, Immunoblot showing KAP1 protein levels in IAPEz-reporter ES cells after KAP1-specific sgRNA introduction and blasticidin selection. Scrambled sgRNA served as control. Blasticidin treatment shows that only cells with successful KAP1 depletion become antibiotic-resistant. Lamin B1 served as loading control. **e**, Flow cytometry dot blot analysis (last 50,000 events) of GFP expression in cells from **d**. Discontinued lines denote GFP-positive threshold. For pseudocolour plots and gating strategy, see Supplementary Fig. 2. KAP1 depletion combined with blasticidin selection leads to IAPEz-reporter reactivation and GFP expression. Experiments in **a**–**e** were replicated at least twice with similar results.

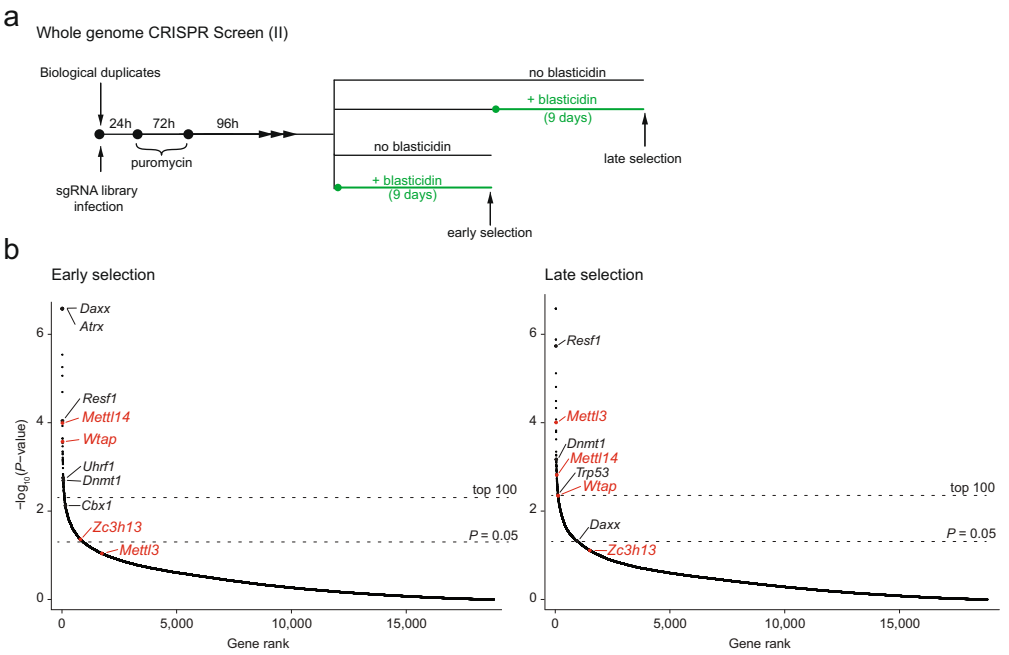

Extended Data Fig. 2 | Early versus late genome-wide CRISPR–Cas9 screen for IAPEz suppressors. a, Schematic of the screening process. **b**, Ranked *P* values (permutation test) for enriched genes in early (left) and late (right) blasticidin treatment, as in **a**. Discontinued lines indicate genes ranked in top 100 according to *P* value (top) and *P* = 0.05 (bottom). Known IAP regulators (black, when $P < 0.05$) and *Mettl3*, *Mettl14*, *Wtap* and *Zc3h13* (red) are reported. Presented data were derived from biological duplicates.

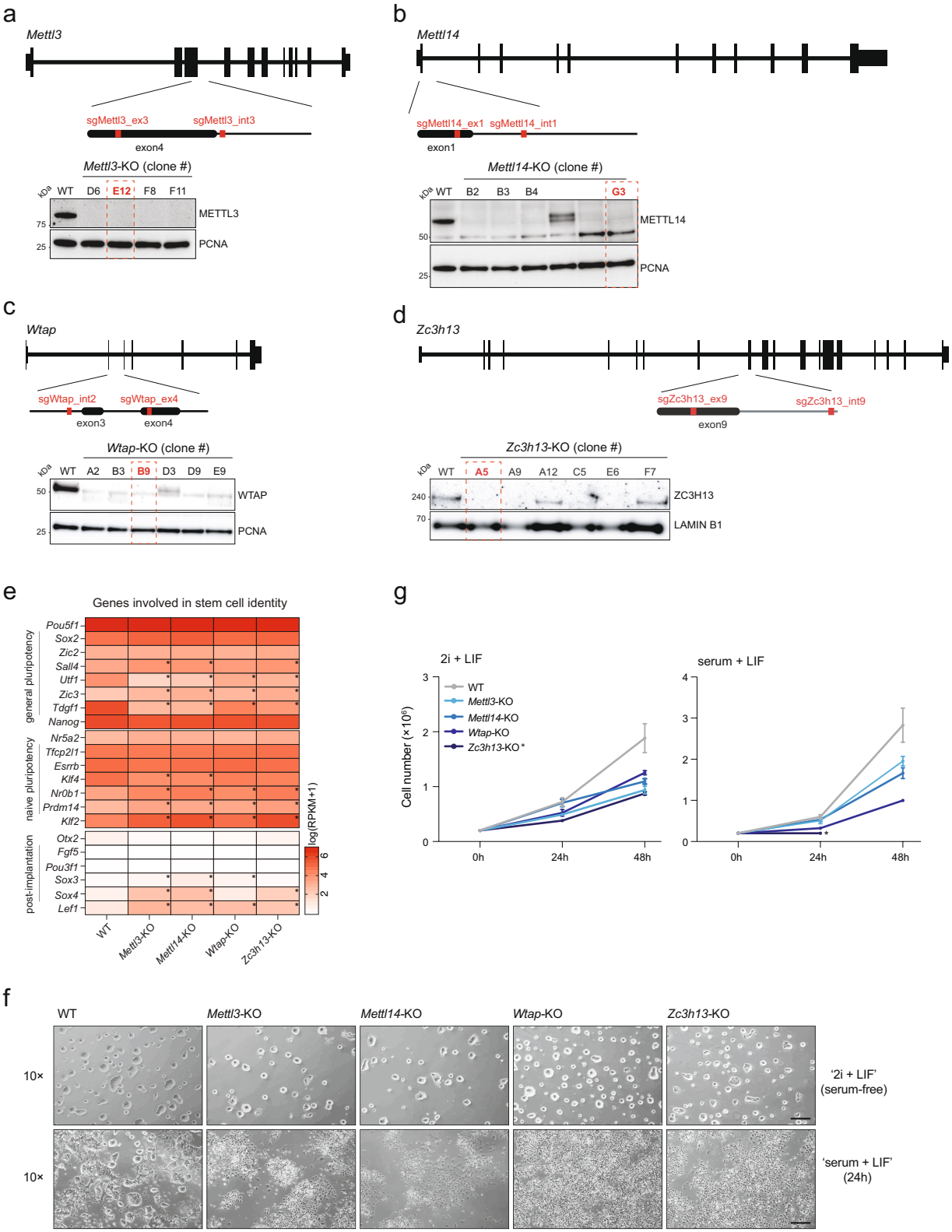

Extended Data Fig. 3 | See next page for caption.

Extended Data Fig. 3 | Generation and validation of *Mettl3-*, *Mettl14-*, *Wtap-* and *Zc3h13*-knockout mouse ES cells. a–**d**, *Mettl3*-knockout (**a**), *Mettl14*-knockout (**b**), *Wtap*-knockout (**c**), and *Zc3h13*-knockout (**d**), mediated by CRISPR–Cas9. Schematic representation showing sgRNAs targeting of indicated loci (top) and immunoblots (bottom) confirming depletion of indicated proteins. PCNA or lamin B1 served as loading controls. In red, clones selected for downstream analyses presented in Figs. 2, 3, Extended Data Figs. 3e–g, 4–7. Western blots for clones indicated in red were repeated at least twice with similar results. **e**, RNA-seq heat maps showing expression of selected pluripotency and post-implantation markers in wild-type, *Mettl3*-knockout, *Mettl14*-knockout, *Wtap*-knockout and *Zc3h13*-knockout ES cells. Asterisks indicate genes with $\log_2$FC > 0.75 and FDR < 0.05. Data represent averages of two independent RNA-seq. **f**, Representative images of wild-type, *Mettl3-*, *Mettl14-*, *Wtap-* and *Zc3h13*-knockout ES cells grown in serum-free 2i + LIF medium, or after 24 h conversion to serum + LIF medium. Scale bar, 0.5 mm. When replacing 2i + LIF with serum + LIF medium, marked morphological changes were observed in all knockout lines. Experiments were repeated twice with similar results. **g**, Growth curves of wild-type, *Mettl3-*, *Mettl14-*, *Wtap-* and *Zc3h13*-knockout ES cells cultured in serum-free 2i + LIF medium, or after conversion to serum + LIF. Data are mean ± s.d. from three independent experiments. When replacing 2i + LIF with serum + LIF medium, the self-renewal ability of *Wtap*-knockout cells was severely impaired and *Zc3h13*-knockout cells disappeared (highlighted by an asterisk). This could explain the lower sgRNA ranking for these two genes upon extended selection time in the screen, which was performed in serum + LIF medium (Extended Data Fig. 2b).

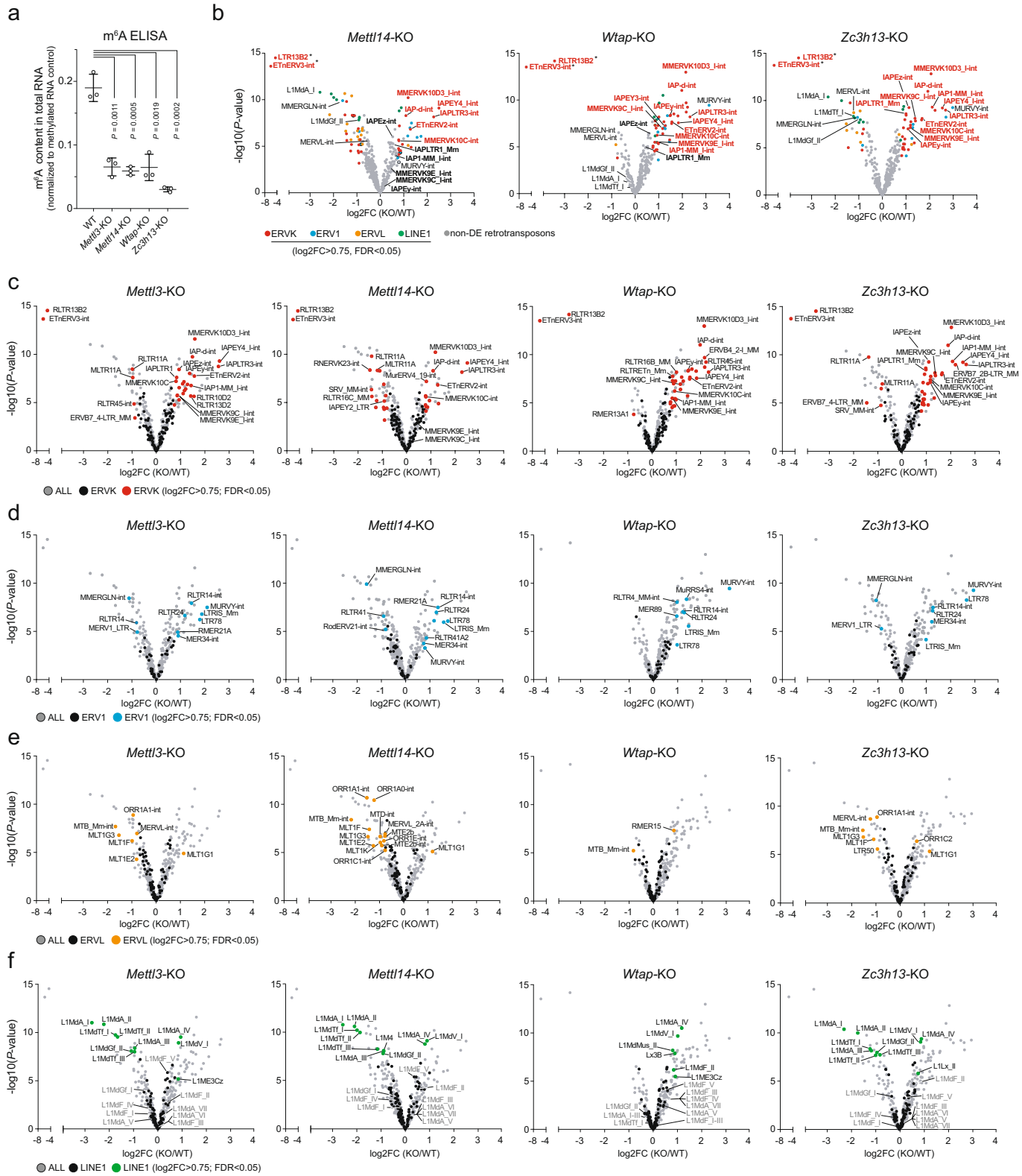

Extended Data Fig. 4 | Depletion of m^{6}A methyltransferase complex results in deregulation of different retrotransposon families. a, ELISA showing normalized m^{6}A levels in total RNA in WT and KO ES cells. Data are mean ± s.d. of three independent RNA samples. *P* values were determined by two-sided Student's *t*-test. **b**, Volcano plot showing $\log_2$FC in retrotransposon expression in *Mettl14*, *Wtap* and *Zc3h13*-knockout versus wild-type cells using a random assignment of multi-mapped reads. In red, blue, orange and green are significantly deregulated RepeatMasker annotations belonging to ERVK, ERV1, ERVL and L1 families, respectively. In grey, non-differentially expressed (non-DE) retrotransposons. *P* values were computed using limma and adjusted with the Benjamini–Hochberg correction (Methods). **c**–**f**, Volcano plots showing $\log_2$FC of retrotransposon expression in *Mettl3*-, *Mettl14*-, *Wtap*- and *Zc3h13*-knockout versus wild-type ES cells using a random assignment of multi-mapped reads. In red, blue, orange and green are significantly deregulated RepeatMasker annotations belonging to ERVK (**c**), ERV1 (**d**), ERVL (**e**) and L1 (**f**) families, respectively ($\log_2$FC > 0.75 and FDR < 0.05). In grey, non-differentially expressed retrotransposons. The *P* values were computed using limma and adjusted with the Benjamini–Hochberg correction.

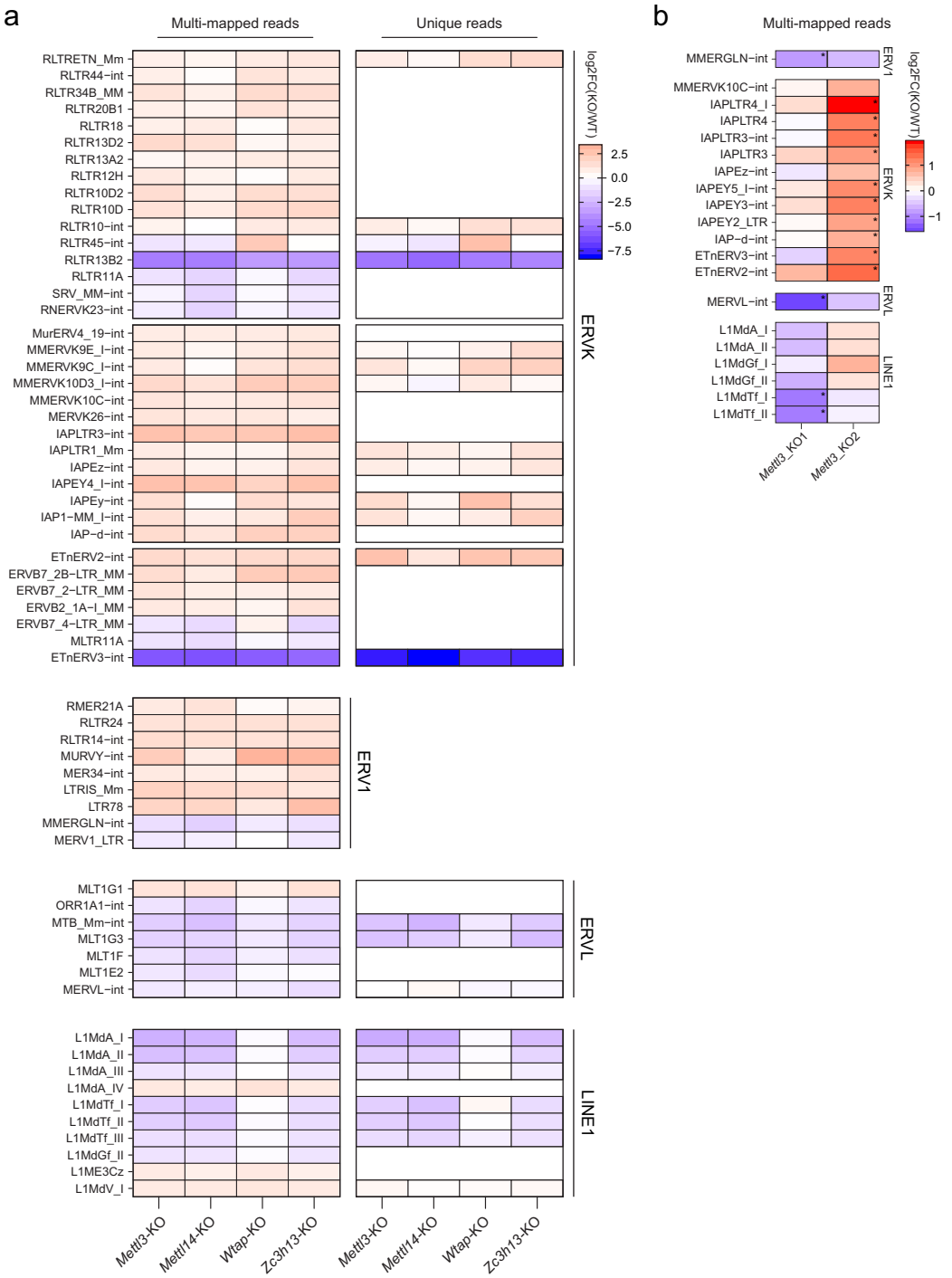

Extended Data Fig. 5 | Family-based analysis of retrotransposon expression using random versus unique mapping. a, RNA-seq heat maps showing log_2FC in expression of indicated retrotransposon families in *Mettl3-*, *Mettl14-*, *Wtap-* and *Zc3h13*-knockout versus wild-type ES cells allowing either multiple mapping with random allocation (left) or unique mapping only (right). In case of unique mappers with intragenic position, only elements transcribed in reverse orientation to the gene were included in the analysis. Note that although ERVK annotations show general upregulation in all knockout ES cells, L1s tended to be downregulated, with the exception of oldest L1MdA_IV, L1ME3Cz and L1MdV_I subfamilies. **b**, Heat maps of published nuclear RNA-seq data[19] showing log_2FC in expression for indicated retrotransposon families in two *Mettl3*-knockout versus control ES cells, allowing multiple mapping with random allocation. The two knockout lines show divergent levels of retrotransposon reactivation but consistently show greater reactivation of ERVK compared to ERVL and LINE1 families. Asterisks indicate retrotransposon families with log_2FC > 0.75 and FDR < 0.05. Data were taken from accession GSE133585.

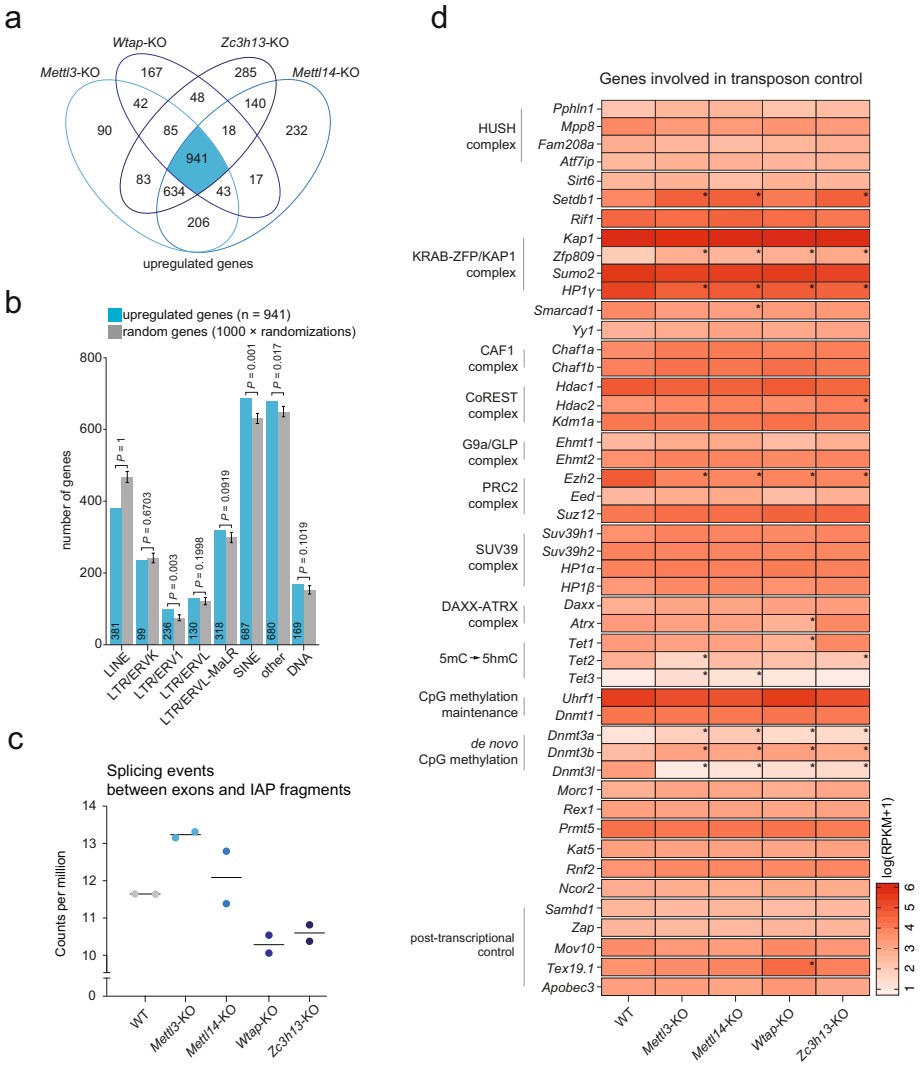

Extended Data Fig. 6 | Analysis of gene expression in mutant ES cells of the m^{6}A methyltransferase complex. a, Venn diagram showing overlap of the upregulated genes (FDR < 0.05, $\log_2$FC > 0.75) in *Mettl3*-, *Mettl14*-, *Wtap*- and *Zc3h13*-knockout ES cells as identified by RNA-seq. In blue, genes ($n = 941$) commonly upregulated in all four knockout ES cells. **b**, Correlation between gene upregulation and proximity to retrotransposon annotations (−5 kb to +1 kb from the TSS). In blue, genes ($n = 941$) commonly upregulated in all four knockout ES cell lines. In grey, random genes plotted as mean + s.d. of $n = 1{,}000$ randomizations. *P* values were determined by permutation test. **c**, Dot plot showing splicing events (normalized counts per million) occurring between exons and RepeatMasker-annotated IAPs in wild-type, *Mettl3*-, *Mettl14*-, *Wtap*- and *Zc3h13*-knockout ES cells. Horizontal lines denote mean ($n = 2$ independent RNA-seq). **d**, Heat map showing average expression of selected retrotransposon regulators in wild-type, *Mettl3*-, *Mettl14*-, *Wtap*- and *Zc3h13*-knockout cells. Genes with $\log_2$FC > 0.75 and FDR < 0.05 are marked by an asterisk.

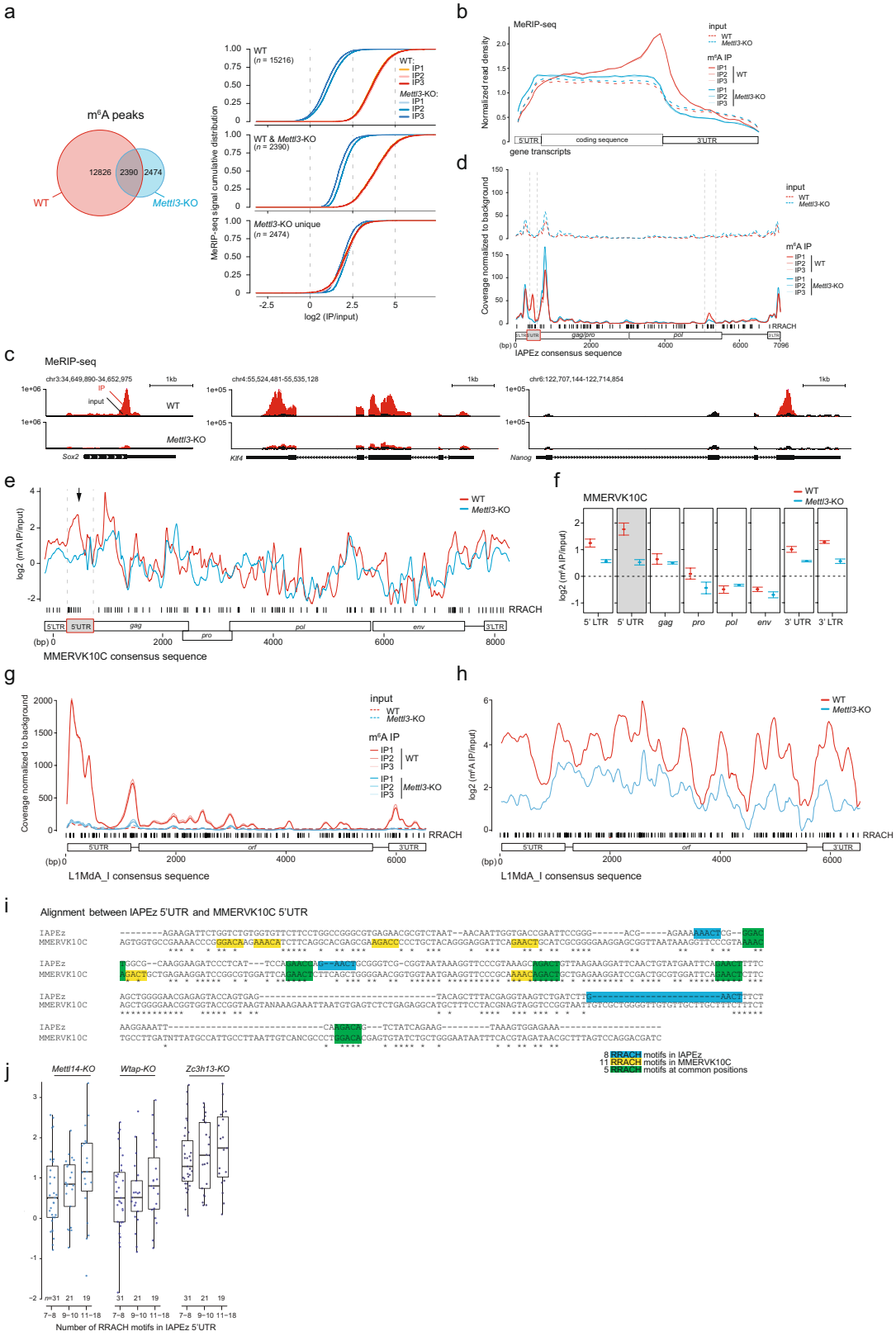

Extended Data Fig. 7 | See next page for caption.

Extended Data Fig. 7 | IAP mRNAs undergo METTL3-dependent m^{6}A methylation. a, Left, Venn diagram showing overlap between m^{6}A peaks identified in wild-type and *Mettl3*-knockout MeRIP-seq. Right, input-normalized cumulative distribution of signal intensity for m^{6}A peaks in wild-type (top), overlapping (middle) and *Mettl3*-knockout specific (bottom) cells. A set of novel m^{6}A peaks was detected in *Mettl3*-knockout cells; however, they are probably false positives (weak signal intensity compared to canonical wild-type peaks). **b**, Normalized MeRIP-seq read density in wild-type (red) and *Mettl3*-knockout (blue) cells across the 5′ UTR, coding sequence and 3′ UTR of mRNA for the genes with at least one m^{6}A peak. Discontinued lines represent respective inputs. **c**, UCSC genome browser tracks showing m^{6}A distribution (red, normalized read density, RPM) at indicated genes in wild-type and *Mettl3*-knockout ES cells. In black, input RNA. Results represent average signal of three independent MeRIP-seq experiments. **d**, Inputs (top) and background-normalized m^{6}A signal distributions (bottom) across the IAPEz consensus sequence in wild-type (red) and *Mettl3*-knockout (blue) cells. Vertical black lines denote positions of RRACH motifs. Discontinued vertical black lines denote regions of m^{6}A enrichment present in wild-type and lost in *Mettl3*-knockout cells. **e**, Average of input-normalized m^{6}A signal intensities along the MMERVK10C consensus sequence in wild-type (red) and *Mettl3*-knockout (blue) cells. Vertical black lines denote RRACH motif positions. Discontinued vertical black lines denote region of m^{6}A enrichment present in wild-type and lost in *Mettl3*-knockout cells. **f**, Average of m^{6}A signal intensities for indicated MMERVK10C sequence segments in wild-type (red) and *Mettl3*-knockout (red) ES cells. Data are mean ± s.d. of three independent MeRIP-seq experiments. **g**, **h**, Background-normalized m^{6}A signal distribution (**g**) and average of input-normalized m^{6}A signal intensities across the L1MdA_I consensus sequence in wild-type (red) and *Mettl3*-knockout (blue) cells (**h**). Vertical black lines denote RRACH motif positions. **i**, Alignment between 5′ UTRs of IAPEz and MMERVK10C consensus sequences. IAP-specific, MMERVK10C-specific and common RRACH motifs are indicated in blue, yellow and green, respectively. **j**, Box plot showing $\log_2$FC in expression of uniquely mapped IAPEz copies grouped according to number of 5′ UTR-associated RRACH motifs in *Mettl14*-, *Wtap*- and *Zc3h13*-knockout versus wild-type cells. Box plots are as in Fig. 2d. Only copies with a minimum of 10 reads in at least one sample were conserved.

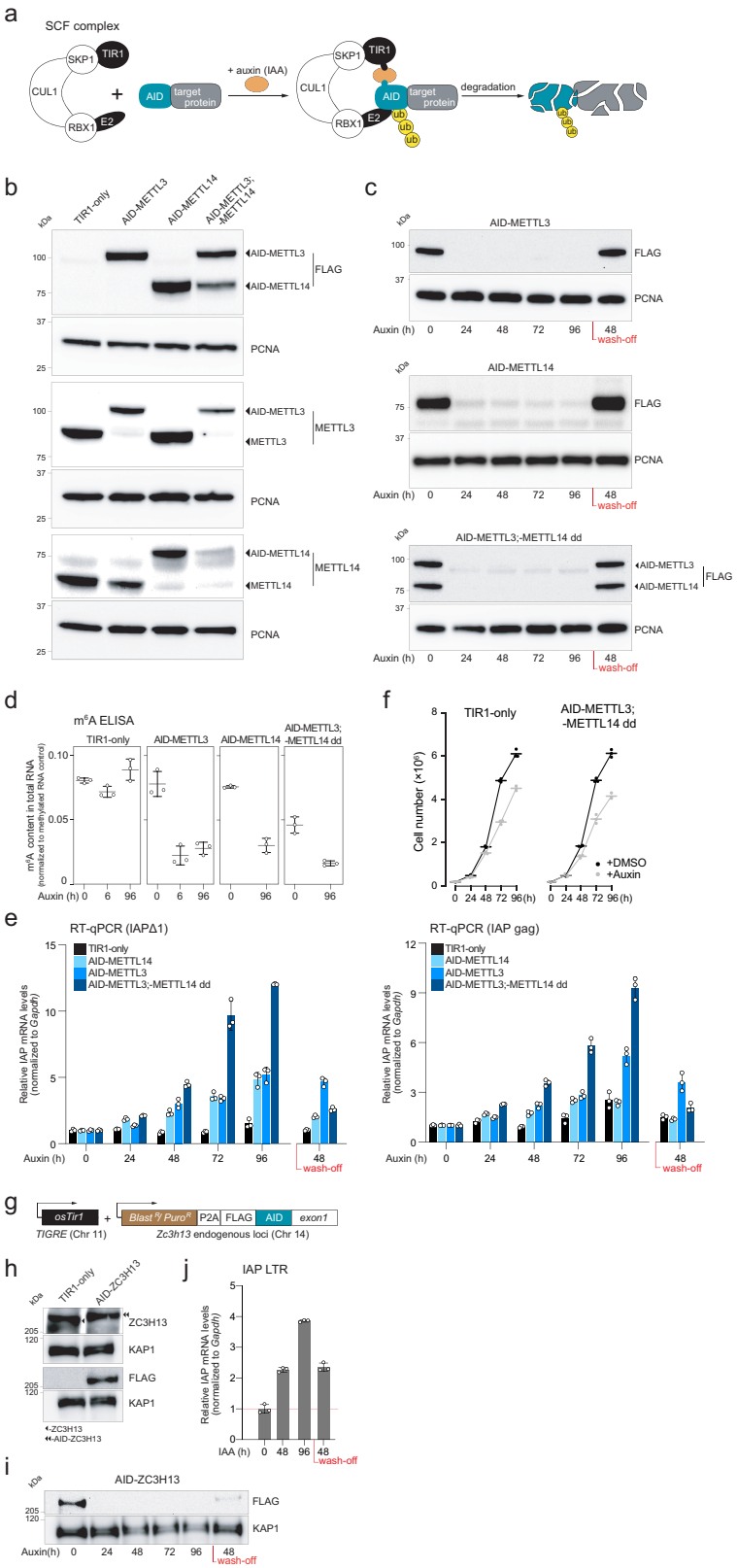

Extended Data Fig. 8 | See next page for caption.

Extended Data Fig. 8 | Auxin-inducible degron of endogenous METTL3, METTL14 and ZC3H13. a, Schematic of TIR1 and SCF1 complex-dependent degradation of endogenously AID-tagged proteins in presence of auxin. **b**, Immunoblot showing protein levels of endogenously 3×Flag-AID-tagged METTL3 and METTL14 in single and double degron ES cell lines. TIR1-only ES cells were used as control for protein levels. PCNA served as loading control. **c**, Immunoblot showing efficiency and reversibility of METTL3 and METTL14 depletion after 0–96 h auxin treatment followed by 48 h auxin wash-off. PCNA served as loading control (related to Fig. 4b). **d**, ELISA showing normalized m^6A levels in total RNA after 0, 6 and 96 h of auxin-induced degradation of METTL3, METTL14 and METTL3;METTL14 double degron. Data are mean ± s.d. of three technical replicates. TIR1-only ES cells served as control. Experiment was repeated twice with similar results. **e**, RT–qPCR showing normalized IAP mRNA levels relative to 0 h using Δ1- or *gag*-specific primers after auxin-induced degradation of METTL14 (light blue), METTL3 (blue) and METTL3;METTL14 double degron (dark blue). TIR1-only (black) ES cells served as control. Data are mean ± s.d. of three independent auxin inductions). **f**, Growth curves of TIR1-only and AID-METTL3;METTL14 double degron ES cells treated with either DMSO (grey) or auxin (black) for 0–96 h. Data are mean ± s.d. of three independent auxin inductions. Note that contrary to constitutive m^6A-knockout ES cells, proliferation rate is not altered by acute m^6A loss (similar rate between AID-METTL3;-METTL14 double degron and TIR1-only ES cells). However, prolonged auxin treatment may have negative effect on the proliferation rate. **g**–**i**, ZC3H13 auxin-dependent degron. Schematic of ZC3H13 degron engineering in mouse ES cells (**g**), immunoblot showing protein levels of endogenously 3×Flag-AID-tagged ZC3H13 (**h**) and degron efficiency in presence of auxin (**i**). TIR1-only ES cells were used as control for protein levels. KAP1 served as loading control. **j**, RT–qPCR showing normalized IAP mRNA levels relative to 0 h using LTR-specific primers after auxin-induced degradation of ZC3H13. Data are mean ± s.d. from three independent auxin inductions. Immunoblots presented in **b**, **c**, **h**, **i** were repeated at least twice with similar results.

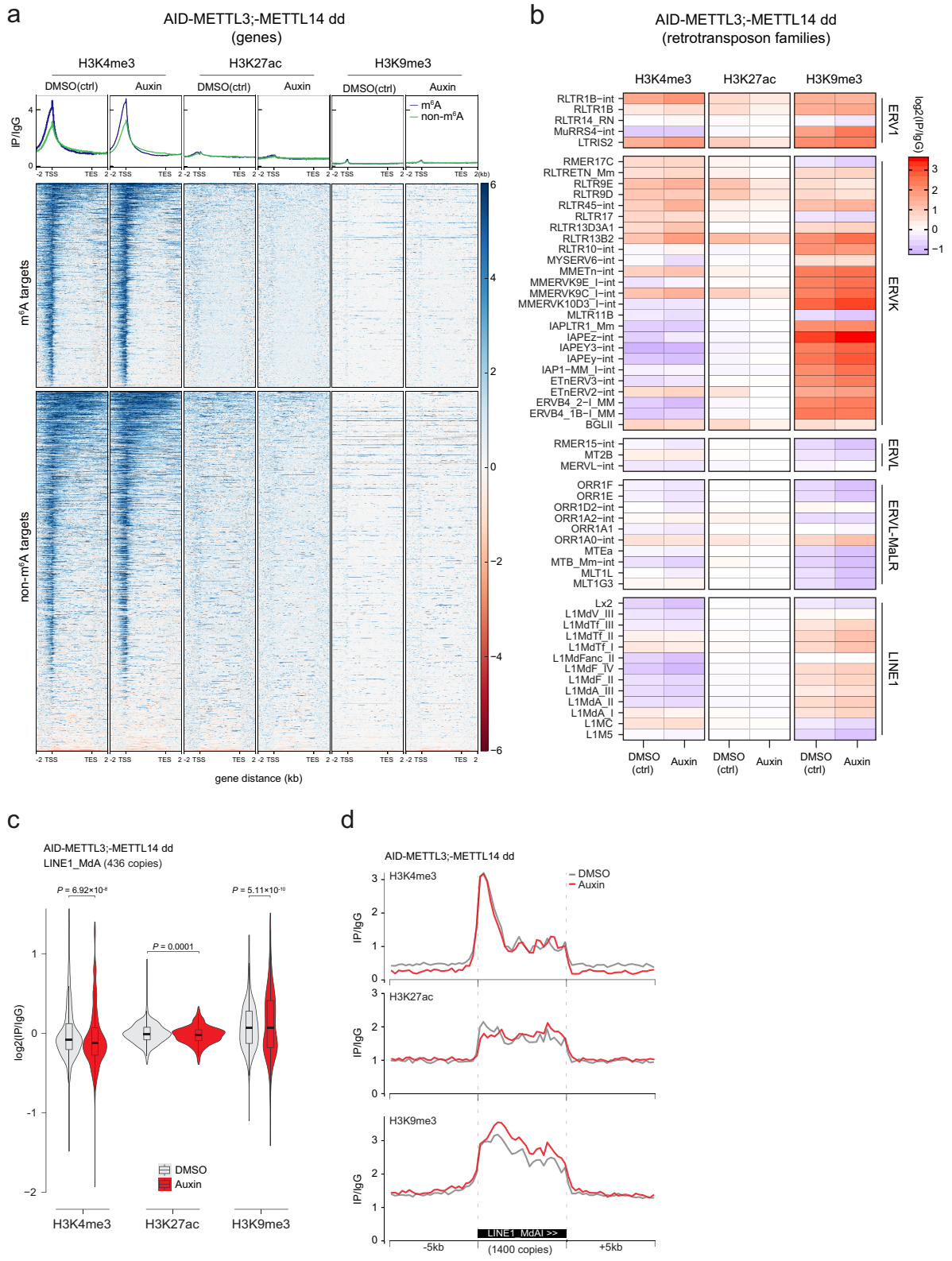

Extended Data Fig. 9 | See next page for caption.

Extended Data Fig. 9 | Retrotransposon chromatin profiling in AID-METTL3;METTL14 double degron ES cells using random assignment of multi-mapped reads on full-length elements. a, Composite profiles (top) and density plots (bottom) showing enrichment of H3K4me3, H3K27ac and H3K9me3 as determined by CUT&RUN on m^{6}A-bound and non-m^{6}A bound genes (±2 kb) (gene lists were obtained based on MeRIP-seq results) in AID-METTL3;METTL14 double degron ES cells treated with DMSO or auxin for 96 h. **b**, Heat map showing average H3K27ac, H3K4me3 and H3K9me3 levels (log_2(immunoprecipitate/IgG)) for 56 retrotransposon families in AID-METTL3;METTL14 double degron ES cells treated with DMSO or auxin for 96 h. **c**, Violin plots and box plots (inside) showing H3K4me3, H3K27ac and H3K9me3 levels at L1MdA_I-IV copies (n = 436 copies) in AID-METTL3;METTL14 double degron ES cells treated with DMSO (grey) or auxin (red) for 96 h. Only copies with a minimum of 10 reads in at least one sample were conserved. Box plots are as in Fig. 2d. P values were determined by two-sided Student's t-test. **d**, Composite profiles showing H3K4me3 (top), H3K27ac (middle) and H3K9me3 (bottom) coverage along full-length (>5 kb) L1MdA_I copies (n = 1,400) in AID-METTL3;METTL14 double degron ES cells treated with DMSO (control, grey) or auxin (red) for 96 h. Results in **a**–**d** represent averages of two independent CUT&RUN.

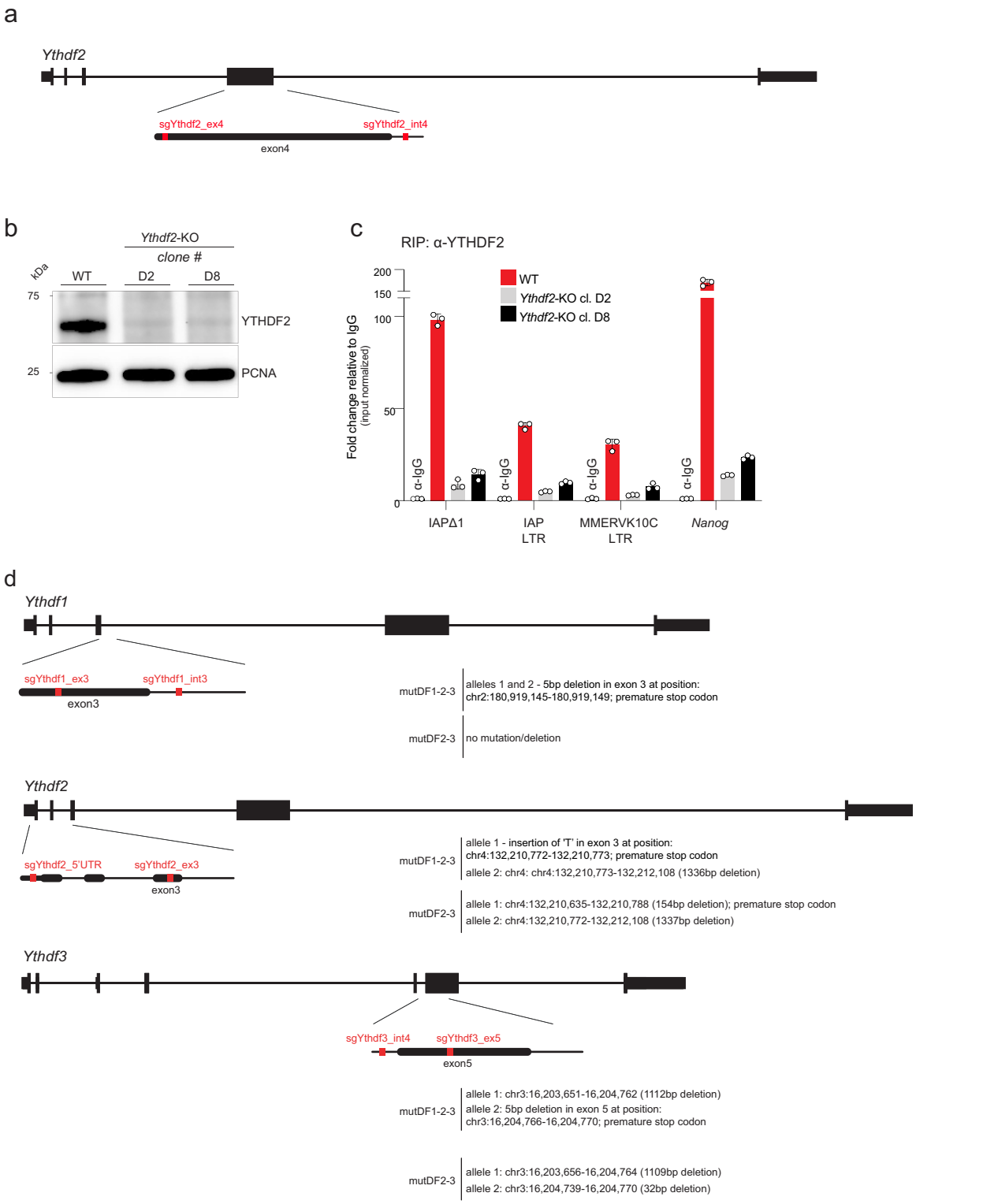

Extended Data Fig. 10 | YTHDF2 binds to ERV mRNAs. a, Schematic representation showing sgRNA targeting of the *Ythdf2* gene. **b**, Immunoblot showing YTHDF2 protein levels in wild-type and YTHDF2-depleted cells. PCNA served as loading control. Immunoblotting was repeated twice with similar results **c**, RIP–qPCR showing YTHDF2 enrichment on indicated ERVKs and *Nanog* in wild-type and *Ythdf2*-knockout ES cells (two independent clones). Rabbit IgG served as control. Data are mean ± s.d. from three independent experiments. **d**, Generation of mutant mut*Ythdf2-3* and mut*Ythdf1-2-3* ES cells using CRISPR–Cas9. Schematic representation showing sgRNA sequences; mutation/deletion information based on Sanger sequencing is provided.

Corresponding author(s): Deborah Bourc'his
Tomasz Chelmicki

Last updated by author(s): Sep 30, 2020

Reporting Summary

Nature Research wishes to improve the reproducibility of the work that we publish. This form provides structure for consistency and transparency in reporting. For further information on Nature Research policies, see Authors & Referees and the Editorial Policy Checklist .

Statistics

For all statistical analyses, confirm that the following items are present in the figure legend, table legend, main text, or Methods section.

n/a	Confirmed	
☐	☒	The exact sample size (*n*) for each experimental group/condition, given as a discrete number and unit of measurement
☐	☒	A statement on whether measurements were taken from distinct samples or whether the same sample was measured repeatedly
☐	☒	The statistical test(s) used AND whether they are one- or two-sided *Only common tests should be described solely by name; describe more complex techniques in the Methods section.*
☒	☐	A description of all covariates tested
☒	☐	A description of any assumptions or corrections, such as tests of normality and adjustment for multiple comparisons
☒	☐	A full description of the statistical parameters including central tendency (e.g. means) or other basic estimates (e.g. regression coefficient) AND variation (e.g. standard deviation) or associated estimates of uncertainty (e.g. confidence intervals)
☐	☒	For null hypothesis testing, the test statistic (e.g. *F*, *t*, *r*) with confidence intervals, effect sizes, degrees of freedom and *P* value noted *Give P values as exact values whenever suitable.*
☒	☐	For Bayesian analysis, information on the choice of priors and Markov chain Monte Carlo settings
☒	☐	For hierarchical and complex designs, identification of the appropriate level for tests and full reporting of outcomes
☒	☐	Estimates of effect sizes (e.g. Cohen's *d*, Pearson's *r*), indicating how they were calculated

Our web collection on statistics for biologists contains articles on many of the points above.

Software and code

Policy information about availability of computer code

Data collection	No costum software was used in this study. Microscopy images were acquired using Upright Spinning disk Confocal Microscope (Roper/ Zeiss). Sequencing data was collected using Illumina HiSeq 2500 and Illumina NovaSeq 6000 Platforms. The qPCR was performed on a ViiA 7 Real-Time QPCR System (Thermo Fisher Scientific). For Western blot, membranes were scanned using a ChemiDoc MP (v.) (BioRad). The FACS analysis was performed using NovoCyte 2000R flow cytometer and NovoExpress Software (v1.2.1) (ACEA Biosciences).
Data analysis	MAGeCK (v0.5.8), Atropos (v1.1.16), STAR (v2.7.0a), One code to find them all (v1.0), featureCounts (v1.5.1), R (v3.5.0), edgeR (v3.22.3), limma (v3.38.3), regioneR (v1.14.0), TrimGalore (v0.4.4), Bowtie (v1.2), deepTools (v2.5.3), MACS2 (v2.1.1), Bowtie2 (v2.2.9), STAR (v2.6.0c), RSAT (v), Picard (v.2.6.0), Trumpet (v0.3.6), TapeStation Controller Software (v3.2), NovoExpress (v1.2.1), Prism (v8.3.0)

For manuscripts utilizing custom algorithms or software that are central to the research but not yet described in published literature, software must be made available to editors/reviewers. We strongly encourage code deposition in a community repository (e.g. GitHub). See the Nature Research guidelines for submitting code & software for further information.

Data

Policy information about availability of data

All manuscripts must include a data availability statement. This statement should provide the following information, where applicable:

- Accession codes, unique identifiers, or web links for publicly available datasets
- A list of figures that have associated raw data
- A description of any restrictions on data availability

All data generated in this study are available on GEO database under the number GSE145616

Field-specific reporting

Please select the one below that is the best fit for your research. If you are not sure, read the appropriate sections before making your selection.

☒ Life sciences ☐ Behavioural & social sciences ☐ Ecological, evolutionary & environmental sciences

For a reference copy of the document with all sections, see nature.com/documents/nr-reporting-summary-flat.pdf

Life sciences study design

All studies must disclose on these points even when the disclosure is negative.

Sample size	Samples size was chosen to ensure reproducibility of the results at affordable costs. Sample size was determined based on previously published studies and equivalent to what is routinely used for respective assay. Sample sizes are indicated for all experiments. At least 2 and typically 3 independent experiments were carried out for most of the assays. For CRISPR-Cas9 knock-out screening, the sample size was determined based on the design as a positive selection strategy and library recommendations. For Screen_I, one pre-selection time point, three selection time points (5-day, 7-day and 9-day long blasticidin S selection) and one non-selection time point (9-day, negative control) were sequenced. Based on the results from Screen I, showcasing increasing selection stringency with extended blasticidin S treatment, independent Screen_II was performed in 2 biological replicates with 9-day long blasticidin S selection following either 8-day long, or 17-day long cell culture (early and late selection respectively). RNA-seq were obtained from biological duplicates. MeRIP-seq was performed in independent triplicates from wildtype and Mettl3-KO cells. Input for each of the cell line was sequenced as a control. CUT&RUN-seq were performed in biological duplicates consistent with comparable studies.
Data exclusions	When experimental mistakes occurred or in case of low sample quality or occasional loss of samples/reagents, the experiment was discarded and repeated. Otherwise, no data were excluded from the analysis.
Replication	All attempts at replication were successful and noted in the relevant figure legends.
Randomization	No randomization techniques were required, as the study was based on molecular and cellular biology techniques, which did not involve live organisms or required allocation of experimental units.
Blinding	The investigators were not blinded to sample allocation during experiments and outcome assessment, because results were obtained using objective quantitative methods.

Behavioural & social sciences study design

All studies must disclose on these points even when the disclosure is negative.

Study description	*Briefly describe the study type including whether data are quantitative, qualitative, or mixed-methods (e.g. qualitative cross-sectional, quantitative experimental, mixed-methods case study).*
Research sample	*State the research sample (e.g. Harvard university undergraduates, villagers in rural India) and provide relevant demographic information (e.g. age, sex) and indicate whether the sample is representative. Provide a rationale for the study sample chosen. For studies involving existing datasets, please describe the dataset and source.*
Sampling strategy	*Describe the sampling procedure (e.g. random, snowball, stratified, convenience). Describe the statistical methods that were used to predetermine sample size OR if no sample-size calculation was performed, describe how sample sizes were chosen and provide a rationale for why these sample sizes are sufficient. For qualitative data, please indicate whether data saturation was considered, and what criteria were used to decide that no further sampling was needed.*
Data collection	*Provide details about the data collection procedure, including the instruments or devices used to record the data (e.g. pen and paper, computer, eye tracker, video or audio equipment) whether anyone was present besides the participant(s) and the researcher, and whether the researcher was blind to experimental condition and/or the study hypothesis during data collection.*
Timing	*Indicate the start and stop dates of data collection. If there is a gap between collection periods, state the dates for each sample cohort.*
Data exclusions	*If no data were excluded from the analyses, state so OR if data were excluded, provide the exact number of exclusions and the rationale behind them, indicating whether exclusion criteria were pre-established.*
Non-participation	*State how many participants dropped out/declined participation and the reason(s) given OR provide response rate OR state that no participants dropped out/declined participation.*

Randomization

If participants were not allocated into experimental groups, state so OR describe how participants were allocated to groups, and if allocation was not random, describe how covariates were controlled.

Ecological, evolutionary & environmental sciences study design

All studies must disclose on these points even when the disclosure is negative.

Study description

Briefly describe the study. For quantitative data include treatment factors and interactions, design structure (e.g. factorial, nested, hierarchical), nature and number of experimental units and replicates.

Research sample

Describe the research sample (e.g. a group of tagged Passer domesticus, all Stenocereus thurberi within Organ Pipe Cactus National Monument), and provide a rationale for the sample choice. When relevant, describe the organism taxa, source, sex, age range and any manipulations. State what population the sample is meant to represent when applicable. For studies involving existing datasets, describe the data and its source.

Sampling strategy

Note the sampling procedure. Describe the statistical methods that were used to predetermine sample size OR if no sample-size calculation was performed, describe how sample sizes were chosen and provide a rationale for why these sample sizes are sufficient.

Data collection

Describe the data collection procedure, including who recorded the data and how.

Timing and spatial scale

Indicate the start and stop dates of data collection, noting the frequency and periodicity of sampling and providing a rationale for these choices. If there is a gap between collection periods, state the dates for each sample cohort. Specify the spatial scale from which the data are taken

Data exclusions

If no data were excluded from the analyses, state so OR if data were excluded, describe the exclusions and the rationale behind them, indicating whether exclusion criteria were pre-established.

Reproducibility

Describe the measures taken to verify the reproducibility of experimental findings. For each experiment, note whether any attempts to repeat the experiment failed OR state that all attempts to repeat the experiment were successful.

Randomization

Describe how samples/organisms/participants were allocated into groups. If allocation was not random, describe how covariates were controlled. If this is not relevant to your study, explain why.

Blinding

Describe the extent of blinding used during data acquisition and analysis. If blinding was not possible, describe why OR explain why blinding was not relevant to your study.

Did the study involve field work? ☐ Yes ☐ No

Field work, collection and transport

Field conditions

Describe the study conditions for field work, providing relevant parameters (e.g. temperature, rainfall).

Location

State the location of the sampling or experiment, providing relevant parameters (e.g. latitude and longitude, elevation, water depth).

Access and import/export

Describe the efforts you have made to access habitats and to collect and import/export your samples in a responsible manner and in compliance with local, national and international laws, noting any permits that were obtained (give the name of the issuing authority, the date of issue, and any identifying information).

Disturbance

Describe any disturbance caused by the study and how it was minimized.

Reporting for specific materials, systems and methods

We require information from authors about some types of materials, experimental systems and methods used in many studies. Here, indicate whether each material, system or method listed is relevant to your study. If you are not sure if a list item applies to your research, read the appropriate section before selecting a response.

Materials & experimental systems

n/a	Involved in the study
☐	☒ Antibodies
☐	☒ Eukaryotic cell lines
☒	☐ Palaeontology
☒	☐ Animals and other organisms
☒	☐ Human research participants
☒	☐ Clinical data

Methods

n/a	Involved in the study
☐	☒ ChIP-seq
☐	☒ Flow cytometry
☒	☐ MRI-based neuroimaging

Antibodies

Antibodies used

Primary antibodes
Antibody, Supplier, Catalog number, Host&Class, Application, Dilution
anti-METTL14, Abcam, ab220030, Mouse monoclonal [CL4252], Western blot, 1:500
anti-METTL3, Abcam, ab195352, Rabbit monoclonal [EPR18810], Western blot, 1:1000
anti-ZC3H13, Invitrogen, PA5-36515, Rabbit polyclonal, Western blot, 1:500
anti-WTAP, Proteintech, 10200-1-AP, Rabbit polyclonal, Western blot, 1:2000
anti-YTHDF1, Proteintech, 17479-1-AP, Rabbit polyclonal, Western blot, 1:1000
anti-YTHDF2, MBL, RN123PW, Rabbit polyclonal, Western blot, 1:1000
anti-YTHDF2, Proteintech, 24744-1-AP, Rabbit polyclonal, RNA Immunoprecipitation (RIP), (4µg/IP)
anti-YTHDF3, Abcam, ab220161, Rabbit monoclonal [EPR21912-3], Western blot, 1:500
anti-PCNA, DAKO, M0879 Mouse monoclonal [PC10] , Western blot, 1:3000
anti-FLAG, Sigma, F1804, Mouse monoclonal [M2], Western blot, 1:1000
anti-KAP1, Abcam, ab10483, Rabbit polyclonal, Western blot, 1:2000
anti-LAMIN B1, Abcam, ab16048, Rabbit polyclonal, Western blot, 1:3000
anti-Cas9, Active motif, 61757, Mouse monoclonal [8C1-F10], Western blot, 1:1000
anti-H3K4me3, Millipore, 07-473, Rabbit polyclonal, Cut@Run, 2µg/experiment
anti-H3K9me3, Abcam, ab176916, Rabbit monoclonal [EPR16601], Cut@Run, 2µg/experiment
anti-H3K27ac, Abcam, ab4729, Rabbit polyclonal, Cut@Run, 2µg/experiment
IgG from Rabbit serum, Sigma, PP54, Cut&Run (2µg/experiment), RIP, (4µg/IP)
IAP-GAG, gift from Dr. Bryan R. Cullen (Duke University School of Medicine, MI, USA), Immunofluorescence (IF), 1:200

Secondary Antibodies
Antibody, Supplier, Catalog Number, Class, Application, Dilution
Goat-anti Mouse IgG (H+L) HRP, Thermo Fisher Scientific, G-21040 polyclonal, western blot 1:10000
Goat-anti Rabbit IgG (H+L) HRP, Thermo Fisher Scientific, G-21234 polyclonal, western blot 1:10000
Goat-anti Rabbit IgG (H+L) Alexa Fluor 488, Thermo Fisher Scientific, A-11008, polyclonal immunofluorescence (IF) 1:500

Validation

Accept anti-IAP-GAG antibody all used antibodies are commercially available and have been validated by manufacturer.
Antibody validations and validation criteria are available on the following websites:
anti-METTL14 https://www.abcam.com/mettl14-antibody-cl4252-ab220030.html
anti-METTL3 https://www.abcam.com/mettl3-antibody-epr18810-ab195352.html
anti-ZC3H13 https://www.thermofisher.com/antibody/product/ZC3H13-Antibody-Polyclonal/PA5-36515
anti-WTAP https://www.ptglab.com/products/WTAP-Antibody-10200-1-AP.htm
anti-YTHDF1 https://www.ptglab.com/products/YTHDF1-Antibody-17479-1-AP.htm
anti-YTHDF2 https://www.mblbio.com/bio/g/dtl/A/index.html?pcd=RN123PW
anti-YTHDF2 https://www.ptglab.com/products/YTHDF2-Antibody-24744-1-AP.htm
anti-YTHDF3 https://www.abcam.com/ythdf3-antibody-epr21912-3-ab220161.html
anti-PCNA https://www.agilent.com/en/product/immunohistochemistry/antibodies-controls/primary-antibodies/proliferating-cell-nuclear-antigen-(concentrate)-76551
anti-FLAG https://www.sigmaaldrich.com/catalog/product/sigma/f1804?lang=fr&region=FR
anti-KAP1 https://www.abcam.com/kap1-antibody-ab10483.html
anti-LAMIN B1 https://www.abcam.com/lamin-b1-antibody-nuclear-envelope-marker-ab16048.html
anti-Cas9 https://www.activemotif.com/catalog/details/61757/cas9-antibody-mab-clone-8c1-f10
anti-H3K4me3 https://www.merckmillipore.com/FR/fr/product/Anti-trimethyl-Histone-H3-Lys4-Antibody,MM_NF-07-473
anti-H3K9me3 https://www.abcam.com/histone-h3-tri-methyl-k9-antibody-epr16601-chip-grade-ab176916.html
anti-H3K27ac https://www.abcam.com/histone-h3-acetyl-k27-antibody-chip-grade-ab4729.html
IgG from Rabbit serum https://www.sigmaaldrich.com/catalog/product/sigma/i5006?lang=fr&region=FR
Goat-anti Mouse IgG (H+L) HRP https://www.thermofisher.com/antibody/product/Goat-anti-Mouse-IgG-H-L-Cross-Adsorbed-Secondary-Antibody-Polyclonal/G-21040
Goat-anti Rabbit IgG (H+L) HRP https://www.thermofisher.com/antibody/product/Goat-anti-Rabbit-IgG-H-L-Cross-Adsorbed-Secondary-Antibody-Polyclonal/G-21234
Goat-anti Rabbit IgG (H+L) Alexa Fluor 488 https://www.thermofisher.com/antibody/product/Goat-anti-Rabbit-IgG-H-L-Cross-Adsorbed-Secondary-Antibody-Polyclonal/A-11008

The anti-IAP-GAG antibody was a kind gift from Dr. Bryan R. Cullen (Duke University School of Medicine, MI, USA) and was described in Dewannieux, M., Dupressoir, A., Harper, F. et al. Identification of autonomous IAP LTR retrotransposons mobile in mammalian cells. Nat Genet 36, 534–539 (2004). https://doi.org/10.1038/ng1353

Eukaryotic cell lines

Policy information about cell lines

Cell line source(s)	All embryonic stem cell lines generated in this study were derived from the a well-characterized E14 mouse embryonic stem cell line. HEK293FT cell line was obtained from Institut Curie CRISPRit Screening Platform.
Authentication	Non of the cell lines were authenticated.
Mycoplasma contamination	ES Cell lines were routinely tested for mycoplasma contamination and tested negative. HEK293FT cell line was not tested for mycoplasma contamination.
Commonly misidentified lines (See ICLAC register)	Cells used are not in the ICLAC database

Palaeontology

Specimen provenance	*Provide provenance information for specimens and describe permits that were obtained for the work (including the name of the issuing authority, the date of issue, and any identifying information).*
Specimen deposition	*Indicate where the specimens have been deposited to permit free access by other researchers.*
Dating methods	*If new dates are provided, describe how they were obtained (e.g. collection, storage, sample pretreatment and measurement), where they were obtained (i.e. lab name), the calibration program and the protocol for quality assurance OR state that no new dates are provided.*

☐ Tick this box to confirm that the raw and calibrated dates are available in the paper or in Supplementary Information.

Animals and other organisms

Policy information about studies involving animals; ARRIVE guidelines recommended for reporting animal research

Laboratory animals	*For laboratory animals, report species, strain, sex and age OR state that the study did not involve laboratory animals.*
Wild animals	*Provide details on animals observed in or captured in the field; report species, sex and age where possible. Describe how animals were caught and transported and what happened to captive animals after the study (if killed, explain why and describe method; if released, say where and when) OR state that the study did not involve wild animals.*
Field-collected samples	*For laboratory work with field-collected samples, describe all relevant parameters such as housing, maintenance, temperature, photoperiod and end-of-experiment protocol OR state that the study did not involve samples collected from the field.*
Ethics oversight	*Identify the organization(s) that approved or provided guidance on the study protocol, OR state that no ethical approval or guidance was required and explain why not.*

Note that full information on the approval of the study protocol must also be provided in the manuscript.

Clinical data

Policy information about clinical studies

All manuscripts should comply with the ICMJEguidelines for publication of clinical research and a completedCONSORT checklist must be included with all submissions.

Clinical trial registration	*Provide the trial registration number from ClinicalTrials.gov or an equivalent agency.*
Study protocol	*Note where the full trial protocol can be accessed OR if not available, explain why.*
Data collection	*Describe the settings and locales of data collection, noting the time periods of recruitment and data collection.*
Outcomes	*Describe how you pre-defined primary and secondary outcome measures and how you assessed these measures.*

ChIP-seq

Data deposition

☒ Confirm that both raw and final processed data have been deposited in a public database such as GEO.

☒ Confirm that you have deposited or provided access to graph files (e.g. BED files) for the called peaks.

Data access links *May remain private before publication.*	https://www.ncbi.nlm.nih.gov/geo/query/acc.cgi?acc=GSE156007

Files in database submission

SuperSeries: GSE145616 m6A methylation regulates the fate of endogenous retrovirus transcripts.
SubSeries:
GSE145309 [RNA-seq]:

GSM4314580 WT ESC_Rep 1
GSM4314581 WT ESC_Rep 2
GSM4314582 Mettl3 KO ESC_Rep 1
GSM4314583 Mettl3 KO ESC_Rep 2
GSM4314584 Mettl14 KO ESC_Rep 1
GSM4314585 Mettl14 KO ESC_Rep 2
GSM4314586 WTAP KO ESC_Rep 1
GSM4314587 WTAP KO ESC_Rep 2
GSM4314588 Zc3h13 KO ESC_Rep 1
GSM4314589 Zc3h13 KO ESC_Rep 2

GSE145315 [RIP-seq]:

GSM4314656 Input_WT
GSM4314657 Input_KO
GSM4314658 m6A_WT_rep1
GSM4314659 m6A_WT_rep2
GSM4314660 m6A_WT_rep3
GSM4314661 m6A_M3KO_rep1
GSM4314662 m6A_M3KO_rep2
GSM4314663 m6A_M3KO_rep3

GSE145615 [CRISPR/Cas9]:

GSM4322248 Screen I_seq1_+puro
GSM4322249 Screen I_seq2_-blast
GSM4322250 Screen I_seq3_blast5D
GSM4322251 Screen I_seq4_blast7D
GSM4322252 Screen I_seq5_blast9D
GSM4322253 Screen II_early_-blast_rep1
GSM4322254 Screen II_early_-blast_rep2
GSM4322255 Screen II_early_+blast_rep1
GSM4322256 Screen II_early_+blast_rep2
GSM4322257 Screen II_late_-blast_rep1
GSM4322258 Screen II_late_-blast_rep2
GSM4322259 Screen II_late_+blast_rep1
GSM4322260 Screen II_late_+blast_rep2

GSE156007 [CUT & RUN]

GSM4718889 Input AID-METTL3:-METTL14 dd (noIAA)
GSM4718890 Input AID-METTL3:-METTL14 dd (+IAA)
GSM4718891 IP:H3K4me3 AID-METTL3:-METTL14 dd (noIAA) Rep1
GSM4718892 IP:H3K4me3 AID-METTL3:-METTL14 dd (noIAA) Rep2
GSM4718893 IP:H3K4me3 AID-METTL3:-METTL14 dd (+IAA) Rep1
GSM4718894 IP:H3K4me3 AID-METTL3:-METTL14 dd (+IAA) Rep2
GSM4718895 IP:H3K27ac AID-METTL3:-METTL14 dd (noIAA) Rep1
GSM4718896 IP:H3K27ac AID-METTL3:-METTL14 dd (noIAA) Rep2
GSM4718897 IP:H3K27ac AID-METTL3:-METTL14 dd (+IAA) Rep1
GSM4718898 IP:H3K27ac AID-METTL3:-METTL14 dd (+IAA) Rep2
GSM4718899 IP:H3K9me3 AID-METTL3:-METTL14 dd (noIAA) Rep1
GSM4718900 IP:H3K9me3 AID-METTL3:-METTL14 dd (noIAA) Rep2
GSM4718901 IP:H3K9me3 AID-METTL3:-METTL14 dd (+IAA) Rep1
GSM4718902 IP:H3K9me3 AID-METTL3:-METTL14 dd (+IAA) Rep2

Genome browser session
(e.g. UCSC)

No web genome browser is available, but an IGV session can be made available upon request.

Methodology

Replicates

CUT@RUN-seq for H3K4me3, H3K27ac and H3K9me3 were performed in biological duplicates for each condition. Single IgG was used as negative control for each condition.

Sequencing depth	For CUT@RUN, on average: 3x in depth, 124 million of sequenced reads (PE50) and 108 million of mapped reads per sample. For precise information on number of sequenced and mapped reads for CUT&RUN-seq, as well as CRISPR-Cas9 screen, RNA-seq and meRIP-seq please see Supplementary Table 5.
Antibodies	Antibody, Supplier, Catalog Number, Host, Class anti-H3K4me3, Millipore, 07-473, Rabbit, polyclonal, anti-H3K9me3, Abcam, ab176916, Rabbit, monoclonal [EPR16601] anti-H3K27ac, Abcam, ab4729, Rabbit, polyclonal IgG from Rabbit serum, Sigma, PP54
Peak calling parameters	Paired-end reads were trimmed using Trim Galore v0.4.4. The alignment was performed onto a concatenated genome using the Mouse reference genome (mm10) and the Escherichia coli genome (str. K-12 substr. MG1655, Genbank: NC_000913) with STAR v2.7.0a35 reporting randomly one position, allowing 6% of mismatches (--outFilterMultimapNmax 5000 --outSAMmultNmax 1 --outFilterMismatchNmax 999 --outFilterMismatchNoverLmax 0.06). PCR duplicates were removed using Picard v2.6.0. Peaks were not called.
Data quality	Quality control (adapters and low-quality bases trimming) was performed using TrimGalore v0.4.4
Software	Trim Galore v0.4.4. STAR v2.7.0a. Picard v2.6.0

Flow Cytometry

Plots

Confirm that:

☒ The axis labels state the marker and fluorochrome used (e.g. CD4-FITC).

☒ The axis scales are clearly visible. Include numbers along axes only for bottom left plot of group (a 'group' is an analysis of identical markers).

☒ All plots are contour plots with outliers or pseudocolor plots.

☒ A numerical value for number of cells or percentage (with statistics) is provided.

Methodology

Sample preparation	Live cells were collected, washed and resuspended in PBS buffer
Instrument	NovoCyte 2000R flow cytometer (ACEA Biosciences).
Software	NovoExpress v1.2.1 (ACEA Biosciences)
Cell population abundance	Minimum of 50,000 cells were counted for each analysis
Gating strategy	The percentage of GFP-positive cells was determined upon definition of three gates: i) FSC-H vs SSC-H to isolate cells from debris,ii) SSC-H vs SSC-A to isolate single cells and iii) SSC-H vs FITC-H for detection of GFP-positive population.

☒ Tick this box to confirm that a figure exemplifying the gating strategy is provided in the Supplementary Information.

Magnetic resonance imaging

Experimental design

Design type	*Indicate task or resting state; event-related or block design.*
Design specifications	*Specify the number of blocks, trials or experimental units per session and/or subject, and specify the length of each trial or block (if trials are blocked) and interval between trials.*
Behavioral performance measures	*State number and/or type of variables recorded (e.g. correct button press, response time) and what statistics were used to establish that the subjects were performing the task as expected (e.g. mean, range, and/or standard deviation across subjects).*

Acquisition

Imaging type(s) — *Specify: functional, structural, diffusion, perfusion.*

Field strength — *Specify in Tesla*

Sequence & imaging parameters — *Specify the pulse sequence type (gradient echo, spin echo, etc.), imaging type (EPI, spiral, etc.), field of view, matrix size, slice thickness, orientation and TE/TR/flip angle.*

Area of acquisition — *State whether a whole brain scan was used OR define the area of acquisition, describing how the region was determined.*

Diffusion MRI ☐ Used ☐ Not used

Preprocessing

Preprocessing software — *Provide detail on software version and revision number and on specific parameters (model/functions, brain extraction, segmentation, smoothing kernel size, etc.).*

Normalization — *If data were normalized/standardized, describe the approach(es): specify linear or non-linear and define image types used for transformation OR indicate that data were not normalized and explain rationale for lack of normalization.*

Normalization template — *Describe the template used for normalization/transformation, specifying subject space or group standardized space (e.g. original Talairach, MNI305, ICBM152) OR indicate that the data were not normalized.*

Noise and artifact removal — *Describe your procedure(s) for artifact and structured noise removal, specifying motion parameters, tissue signals and physiological signals (heart rate, respiration).*

Volume censoring — *Define your software and/or method and criteria for volume censoring, and state the extent of such censoring.*

Statistical modeling & inference

Model type and settings — *Specify type (mass univariate, multivariate, RSA, predictive, etc.) and describe essential details of the model at the first and second levels (e.g. fixed, random or mixed effects; drift or auto-correlation).*

Effect(s) tested — *Define precise effect in terms of the task or stimulus conditions instead of psychological concepts and indicate whether ANOVA or factorial designs were used.*

Specify type of analysis: ☐ Whole brain ☐ ROI-based ☐ Both

Statistic type for inference (See Eklund et al. 2016) — *Specify voxel-wise or cluster-wise and report all relevant parameters for cluster-wise methods.*

Correction — *Describe the type of correction and how it is obtained for multiple comparisons (e.g. FWE, FDR, permutation or Monte Carlo).*

Models & analysis

n/a	Involved in the study
☐	☐ Functional and/or effective connectivity
☐	☐ Graph analysis
☐	☐ Multivariate modeling or predictive analysis

Functional and/or effective connectivity — *Report the measures of dependence used and the model details (e.g. Pearson correlation, partial correlation, mutual information).*

Graph analysis — *Report the dependent variable and connectivity measure, specifying weighted graph or binarized graph, subject- or group-level, and the global and/or node summaries used (e.g. clustering coefficient, efficiency, etc.).*

Multivariate modeling and predictive analysis — *Specify independent variables, features extraction and dimension reduction, model, training and evaluation metrics.*